# Chapter 3

## Spiramycin

### 3.1 Introduction

The macrolide antimicrobial family comprised 14, 15 and 16 member-ringed compounds that are characterised by a macrocyclic lactone ring with various amino sugars attached. Macrolides form a distinct group of antimicrobials that are closely related in terms of chemical structure, resistance and mechanism of action but varies in pharmacokinetic parameters and spectrum of activity (Jain & Danziger, 2004).

The first macrolide drug, erythromycin, was isolated in 1952 from *Streptomyces erythreus* by McGuire *et al*. (1952) and is the prototype drug from which the newer derivatives are synthesised (Jain & Danziger, 2004; Chambers, 2007). Despite its success over the past decades, erythromycin has limitations, a high dosage frequency, distressing gastro-intestinal side-effects and reduced bioavailability after exposure to gastric acid. A new generation of macrolides has since been developed to improve the spectrum of activity and decrease adverse effects (Kanatani & Guglielmo, 1994).

Spiramycin is a mixture of three components namely spiramycin I, which has a hydroxyl group at C-3 of aglycine; spiramycin II, in which the hydroxyl group is acetylated; and spiramycin III, in which the same position is propionylated (Ikeda & Kitao, 1979). This 16-membered macrolide is mainly produced by certain strains of *Streptomyces ambofaciens,* where it is harvested from the broths through solvent extraction (Shi *et al.,* 2006).

Spiramycin is of particular significance because of its efficacy against bacteria that have acquired resistance to erythromycin and other macrolides. Also the lack of major side-effects makes spiramycin a safer alternative (Rubinstein & Keller, 1998).

## 3.2 Description and nomenclature

### 3.2.1. Chemical name

Spiramycin I. The main component is (4*R*,5*S*,6*S*,7*R*,9*R*,10*R*,11*E*,13*E*,16*R*)-6-[[3,6-dideoxy-4-*O*-(2,6-dideoxy-3-*C*-methyl-α-L-*ribo*hexopyranosyl)-3-(dimethylamino)-β-D-glucopyranosyl]oxy]-4-hydroxy-5-methoxy-9,16-dimethyl-7-(2-oxoethyl)-10-[[2,3,4,6-tetradeoxy-4-(dimethylamino)-D-*erythro*-hexopyranosyl]oxy]oxacyclohexadeca-11,13-dien-2-one.

Spiramycin II (4-*O*-acetylspiramycin I) and spiramycin III (4-*O*-propanoylspiramycin I) are also present (BP *(Vet)* 2012).

### 3.2.2. Non-proprietary name

Spiramycin

### 3.2.3 Proprietary names

Acetylspiramycin®, Dicorvin®, Osmycin®, Rovadin®, Rovamicina®, Rovamycin®, Rovamycin Forte®, Rovamycine®, Rovamycin® [inj.], Selectomycin®, Spirabiotic®, Spiradan®, Spiranter® (Merck Manual, 2011).

### 3.3 Formulae

#### 3.3.1 Structural formula

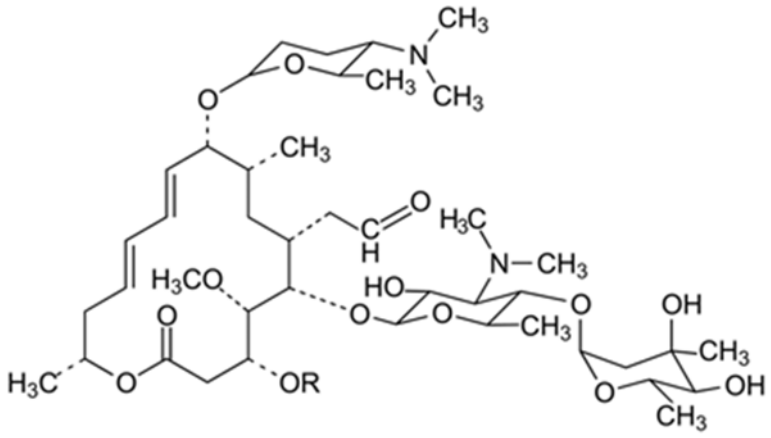

**Figure 3.1** Structural formula of spiramycin (Medicines complete, 2010).

**Table 3.1** Structural information of spiramycin (BP (*Vet*) 2012)

| Compound | R | Molecular Formula | $M_r$ |
|---|---|---|---|
| Spiramycin I | H | $C_{43}H_{74}N_2O_{14}$ | 843.1 |
| Spiramycin II | CO-$CH_3$ | $C_{45}H_{76}N_2O_{15}$ | 885.1 |
| Spiramycin III | CO-$CH_2$-$CH_3$ | $C_{46}H_{78}N_2O_{15}$ | 899.1 |

### 3.4 Physical properties

#### 3.4.1 Appearance and colour

White or slightly yellowish amorphous powder, slightly hygroscopic (BP (*Vet*) 2010; Medicines complete, 2010).

#### 3.4.2 Solubility

Spiramycin is slightly soluble in water, freely soluble in acetone, in ethanol (96 per cent) and in methanol (BP *(Vet)* 2012).

### 3.5 Pharmacology

#### 3.5.1 Mode of action

The mechanism of action of spiramycin has not yet been elucidated fully. However, there is considerable evidence that its antibacterial activity is a result of reversible binding to the 50S ribosomal unit, causing blockage of the transpeptidation or translocation reactions, inhibiting protein synthesis and subsequent cell growth (Brisson-Noël *et al.,* 1988; Smith, 1988; Reynolds, 1993). Although macrolides are primarily bacteriostatic, they may in high concentrations be bactericidal against more susceptible strains (Brisson-Noël *et al.,* 1988).

#### 3.5.2 Therapeutic activity

Spiramycin has a considerable therapeutic activity as (i) it concentrates within the body cells from where it is gradually released; (ii) it stimulates the body's immune system against pathogens, exerting a probiotic effect and (iii) it displays evidence of substantial post-antibiotic effects (Rubinstein & Keller, 1998).

The antibacterial spectrum of spiramycin is, like the other macrolides, quite broad, encompassing most pathogens involved in respiratory tract infections. These include gram-positive and gram-negative cocci, Parvobacteriaceae, *Legionalla* spp., *Chlamydia* spp., *Urea plasma urealyticum*, *M*. *pneumonia* and *Lysteria monocytogenes*, but exclude Enterobacteria (Brook, 1998; Rubinstein & Keller, 1998). Spiramycin displays similar activity against *S*. *pneumonia* when compared to other macrolides and its parent compound, erythromycin. Studies have shown that strains with inducible resistance against erythromycin are *in vitro* still susceptible to this 16-membered macrolide. Conventional MIC tests performed *in vitro* have shown borderline activity against *Haemophilus influenza* whilst *in vivo* tests showed that spiramycin still maintained its activity against this organism (Rubinstein & Keller, 1998).

Spiramycin is used as an alternative treatment for toxoplasmosis during pregnancy. Although the combination of pyrimethamine and sulphadiazine is the treatment of choice, spiramycin is not teratogenic and is therefore not considered harmful to the mother, fetus or newborn. The transmission from mother to fetus is also lowered (Stray-Pederson, 1992). The anti-inflammatory and membrane stabilising effects of the 14- and 15-member macrolides and ketolides are well established (Perry *et al*., 1992; Anderson *et al*., 1996; Feldman *et al*., 1999). However, spiramycin and jocamycin lack the inhibitory effects on the generation of pro-inflammatory, toxic reactive oxidants by neutrophils. This can be ascribed to the weak membrane-stabilising effects of these two agents (Theron *et al.,* 2000).

### 3.5.3 Dosage

Dosing of spiramycin may be expressed as either milligrams (mg) or International Units (IU). One mg of spiramycin is equivalent to approximately 3000 IU (Reynolds, 1993).

#### 3.5.3.1 Antibacterial

##### 3.5.3.1.1 Usual adult and adolescent dose

Oral, 1 to 2 grams (3,000,000 to 6,000,000 IU) two times a day; or 500 mg to 1 gram (1,500,000 to 3,000,000 IU) three times a day. For severe infections, the dose may be increased to 2 to 2.5 grams (6,000,000 to 7,500,000 IU) two times a day (Reynolds, 1993; Drugspedia, 2007)

##### 3.5.3.1.2 Usual paediatric dose

Children 20 kg of body weight and over: Oral, 25 mg (75,000 IU) per kg of body weight two times a day, or 16.7 mg (50,000 IU) per kg of body weight three times a day (Reynolds, 1993; Drugspedia, 2007).

### 3.5.4 Adverse reactions

Frequency not defined:

- dermatologic: angioedema (rare), pruritus, rash, urticaria
- gastrointestinal: diarrhoea, nausea, pseudomembranous colitis (rare), vomiting
- hepatic: transaminases increased
- neuromuscular & skeletal: paresthesia (rare)
- miscellaneous: anaphylactic shock (rare)

Rare adverse reactions associated with other macrolide antibiotics include life-threatening ventricular arrhythmia, prolongation of $QT_c$, and neuromuscular blockade (Merck Manual, 2011).

### 3.6 Pharmacokinetics

#### 3.6.1 Absorption

The most common route of administration is the oral route, but spiramycin adipate intravenous infusion can also be given. In an investigation into the bioavailability of spiramycin, the absolute bioavailability between different doses varied slightly whilst wide inter-individual variations for different doses were noted. From this information the absolute bioavailability of spiramycin was determined to be generally in the range of 30-40%. Significant variations in serum concentrations of spiramycin were also observed (Frydman *et al*., 1988).

The rate of absorption for spiramycin seems to be quite slow in comparison with erythromycin and other agents. The time needed to reach $C_{max}$ in healthy volunteers was 3 hours after administering a 1 g oral dose of spiramycin. The reason for its slow rate of absorption may be related to its high $pK_a$ value of 7.9, suggesting a high degree of ionisation in the acidic environment of the stomach. However, spiramycin does not show any signs of chemical breakdown in low pH environments and therefore appears to be stable in the stomach (Kamme *et al*., 1978). Studies have shown that co-administration of food delays the time to reach peak concentration (from 4h to 6h) and significantly reduces the bioavailability (by 50%) (Frydman *et al*., 1988).

#### 3.6.2 Distribution

Macrolides, in contrast to β-lactams and aminoglicosides, have extensive tissue distribution in both humans and animals (Frydman *et al*., 1988). In experimental findings the Vd at steady state ($V_{ss}$) of spiramycin was well in excess of total body water, at 383L, versus 18-20L for aminoglicosides and 20-25L for penicillins and cephalosporins. This has considerable therapeutic implications since it suggests that spiramycin can also penetrate tissue and cells and is not limited to the extracellular fluid (Wise, 1993).

#### 3.6.3 Metabolism

Studies indicate that spiramycin is metabolised in the liver to active metabolites, from where a substantial amount is excreted in the bile and approximately 10% in the urine (Martindale, 2012). Several macrolides, in particular erythromycin salts and triacetyloleandomycin, have shown to impair cytochrome P450-dependent pathways of liver microsomal drug oxidation processes (Descotes *et al.,* 1988). Spiramycin, on the other hand does not seem to have

the same ability to depress cytochrome P450 activity, as suggested by its lack of interaction with other drugs including theophylline and antipyrine. However, this needs to be studied further (Descotes *et al*., 1988).

### 3.6.4 Excretion

The excretion of spiramycin appears to be mainly via non-renal routes (i.e. biliary). A study found that 4.4% of a spiramycin dose was eliminated after 24 hours through this route (Kavi *et al*., 1988). Other investigators conducted urine tests, where the mean figure of 14% of the drug was detected 48 hours after it had been administered (Frydman *et al*., 1988).

The total body clearance after a 500 mg intravenous dose of spiramycin was determined to be 1.14 L/min (Frydman *et al*., 1988). The fact that this value is similar to that of liver blood flow suggests that spiramycin is actively secreted by non-renal processes. Test subjects that received an oral dose of 500 mg three times daily achieved rapid biliary concentrations of spiramycin (60 mg/L) (Inoue & Deguchi, 1982). The serum elimination half-life of spiramycin is between 6.2 and 7.7 h (Wise, 1993).

## 3.7 Pharmacodynamics

### 3.7.1 Tissue penetration

The area under the serum concentration curve following intravenous infusion of spiramycin indicates extensive tissue distribution. As depicted in figure 3.2, after the peak concentration attained at the end of a one-hour infusion, there is a marked drop in the concentration as drug distribution takes place, followed by a slower elimination phase after 3 to 4 hours (Frydman *et al*., 1988).

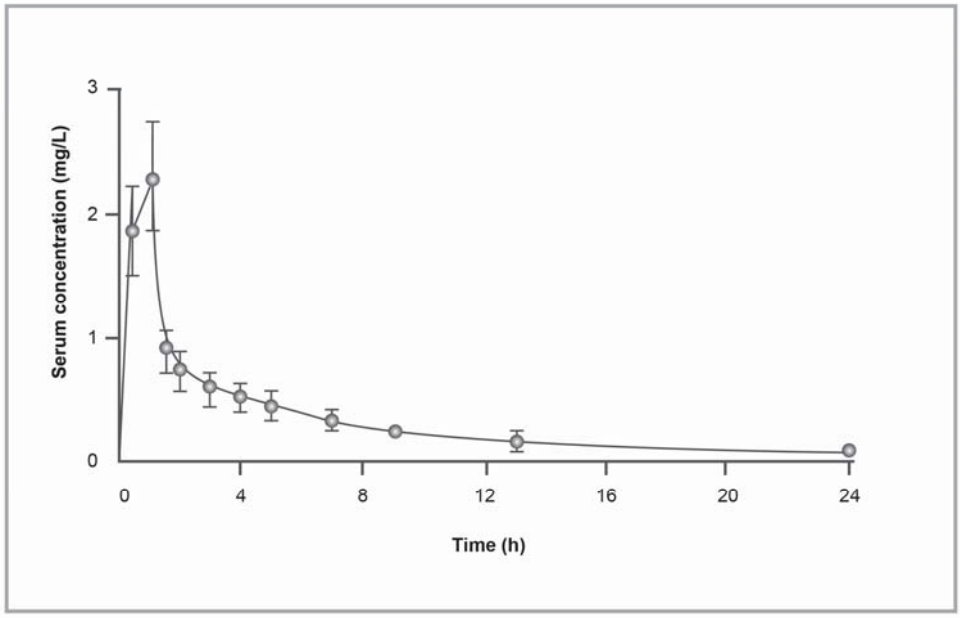


**Figure 3.2** Mean (± standard deviation) serum concentration of spiramycin in 34 healthy young volunteers after 1-hour infusion of a single 500 mg dose (Wise, 1993).

Table 3.2 shows the concentration of spiramycin achieved in human tissue and fluids after oral administration. What is of particular interest is the ability of spiramycin to achieve high concentrations at various sites in the respiratory tract. Results from the administration of 2 to 3 g twice daily showed high concentrations in healthy lungs, atelectatic lung tissue and bronchial mucosa. The concentration in healthy lungs 18 hours after administration was 19 to 48 mg/kg, 20 to 60 mg/kg in atelectatic lungs and 16 to 36 mg/kg in bronchial mucosa. This indicates that spiramycin persists for long periods of time in the lung tissue (Brook, 1998).

**Table 3.2** Spiramycin concentrations achieved in human tissues and fluids (Brook, 1998)

| **Tissue** | **Oral dosage (dose/day × days)** | **Time since dose** | **Tissue concentration (mg/kg)** |
|---|---|---|---|
| Serum | 3.75 (sd) | 12 | 1.5 |
| Prostate | 2 g × 16 | 13 | 21 |
| | 3 g × 10 | 240 | 1.7 |
| Muscle | 2 g × 16 | 12 | 27 |
| Bone | 1 g | 12 | 5.3 |
| | 3 g × 10 | 240 | 1.7 |
| Spleen | 3 g × 10 | 240 | 6.8 |
| Liver | 3 g × 10 | 240 | 5.9 |
| Kidney | 3 g × 10 | 240 | 6.1 |
| Lung | 3 g × 10 | 240 | 1.5 |
| Lung healthy | 3 g × 2 | 18 | 45 ± 18 |
| | 3 g × 2 | 18 | 30 ± 16.2 |
| Bronchial secretion | 1 g × 2 | 1 | 22 (serum 0.12) |
| | 1 g × 2 | 6 | 6 (serum 0.34) |
| Tonsil and adenoids | 3 g (sd) | | 29.5 |
| Tonsil | 100 mg/kg (sd) | 36 | 45.3 |
| | 100 mg/kg (sd) | 84 | 2.5 |

*Abbreviation:* sd = single dose

The site of infection-to-serum ratio can give a good indication of the degree to which an antimicrobial agent concentrates in the cellular component (Baldwin *et al.,* 1992). In table

3.3 the site of infection-to-serum ratio for a number of antimicrobial agents in the lung tissue is given including spiramycin which has the highest value by some margin (Brook, 1998).

**Table 3.3** Selected site of infection-to-serum ratios for whole lung tissue (Brook, 1998)

| **Antimicrobial agent** | **Site of infection-to-serum ratio** |
|---|---|
| amoxicillin | 0.40 - 0.49 |
| clavulanate | 0.23 |
| floxacillin | 0.16 - 0.36 |
| cefamandole | 0.39 - 0.52 |
| doxycycline | 2.3 |
| amikacin | 0.5 |
| tobramycin | 0.5 |
| erythromycin | 1.7 - 5 |
| spiramycin | 2.2 - 38 |

Spiramycin has also shown to have good diffusion into various pelvic tissues. Concentrations in the fallopian tubes were the highest, ranging from 4.4 to 33 mg/kg, while concentrations in the ovaries, myometrium and vaginal mucosa exceeded plasma concentrations (Allen *et al*., 1988). This emphasises the potential role of this agent in the treatment of pelvic inflammatory disease, a disorder where a wide range of organisms is implicated that are known to be susceptible or at least partially susceptible to spiramycin (Brook, 1998).

### 3.7.2 Intracellular penetration

Intracellular pathogens that respond in varying degrees to macrolide treatment include: *Legionella*, *Mycoplasma* and *Chlamydia* spp (Wise, 1993). For macrolides to exert their bactericidal effect enough of the antibiotic must accumulate within the infected cells. It appears that the transport and delivery of the antibiotic to the site of action may be influenced by the presence phagocytes and a synergy exists between the antibiotic present

in the cells and the natural bactericidal activity of the polymorponuclear leukocytes (Pocidalo *et al.*, 1985; Veber *et al.,* 1993).

High intracellular concentrations were measured in alveolar macrophages and human bronchoalveolar lavage supernatant. These concentrations exceeded simultaneous serum concentration 10- to 20-fold, supporting the overall effectiveness of spiramycin in the treatment of susceptible pathogens responsible for pulmonary infections (Harf *et al.*, 1988).

Spiramycin and erythromycin produced similar polymorphonuclear neutrophil concentrations measured 3 hours after equal doses were administered but spiramycin resided much longer in these cells when compared to erythromycin, which is probably the reason for its prolonged half-life (Pocidalo *et al.*, 1985).

### 3.7.3 Post-antibiotic effect

The post-antibiotic effect can be defined as the continued inhibition of bacterial growth after limited exposure to an antimicrobial agent after the antibiotic is removed (Brook, 1989). Macrolides, in contrast to β-lactams, display an evident PAE against both Gram-negative and Gram-positive bacteria. Spiramycin, like other 16-membered ring macrolides, have a more marked PAE which is proportional to the time of exposure and concentration. A pronounced inhibitory effect against *S. aureus* was observed in spiramycin in comparison to the parent compound. After a 3 hour exposure of 4 times the minimal inhibitory concentration, the PAE of erythromycin was 5 hours versus the 9 hours resulting from exposure to spiramycin (Webster *et al.,* 1988).

### 3.7.4 Inhibitory quotient

Inhibitory quotient is the ratio between measured concentration of an antibiotic in a particular tissue or body fluid to the MIC of a pathogen. Studies have shown that spiramycin has a high inhibitory quotient for many common respiratory pathogens, even for pathogens with high MIC values (Brook, 1998).

### 3.7.5 Residential time

A study done by Bergogne-Berezin (1988) showed that the half-life of (t½) of spiramycin is much longer than that of other macrolides. The concentration of macrolides in infected lungs of 2 different mice was measured. Investigators found that t½ for spiramycin was 24 hours, compared with 6 and 8 hours for erythromycin and roxithromycin respectively. The survival

rate of the mice subjected to the spiramycin regimen was notably higher than with the other macrolides used in this study (Bergogne-Berezin, 1996).

### 3.8 The physico-chemical properties of spiramycin

The literature states that spiramycin is formulated as an amorphous powder. In an article by Craig *et al*. (1999) concerning the relevance of the amorphous state and its impact on pharmaceutical dosage form and design, emphasis was placed on the molecular processes associated with glass transitional behaviour and thermal methods for characterising the glass transition temperature ($T_g$). Also mentioned is the lack of "comfort factor" associated with the use of amorphous systems, since structural characterisation and quality control of these systems are much more difficult with reference to the crystalline state. Similarly, the exact relationships between glass transition temperature $T_g$ and pharmaceutical product performance are not yet fully understood. It is these difficulties that have in many instances led to the rejection of the amorphous drug form as a formulation strategy, even though it offers a potential means to improve product performance considerably.

The characterisation of spiramycin presented a unique challenge since conventional methods including the use of thermal and spectroscopic methods are often not considered as reliable techniques for characterisation of amorphous substances. Also, the structure and energy levels seem to be changing constantly through a process called structural relaxation (section 1.6.4) (Cui, 2007).

### 3.9 Recrystallisation method

Spiramycin powder was added to a glass beaker containing a small volume of organic solvent. The beaker was placed on a hot plate (Heidolph, Germany) where it was heated to just below the boiling point of the solvent. Additional solvent was gradually added to the solution, whilst stirring continuously with a magnetic stirrer, until supersaturation was achieved. The supersaturated solutions were covered with pierced Parafilm® and left undisturbed at room temperature to allow recrystallisation to take place through the gradual evaporation of solvent.

The slow evaporation technique failed to produce any crystalline products. Instead, it yielded a highly viscous resin-like substance, with no definitive morphological shape. In time this viscous mass solidified to a glassy, amber-like substance which in turn reverted back to an amorphous powder once all of the solvent had evaporated. The SEM photomicrographs

and X-ray results later confirmed the amorphous character of the raw material and the recrystallisation products. Methods discussed in chapter 2 were implemented to characterise and predict the stability of spiramycin.

## 3.10 Results

### 3.10.1 Spiramycin raw material

**Differential scanning calorimetry (DSC)**

DSC analysis was performed on samples weighing approximately 3-6 mg in pierced aluminium crimp cells. The samples were heated to a maximum temperature of 200ºC at a heating rate of 10ºC/min under a nitrogen purge flow of 35 ml/min.

Figure 3.3 shows the DSC thermogram of the amorphous spiramycin raw material, with the endothermic event at 116.7ºC representing the glass transition point ($T_g$) (section 1.6.1), accompanied by the loss of heat capacity, followed by a recovery in the baseline at 119.5ºC, signalling the end set of the event. In this instance the $T_g$ was much easier to observe as this was a one-component system, containing none of the residual solvent that were present in all of the other samples.

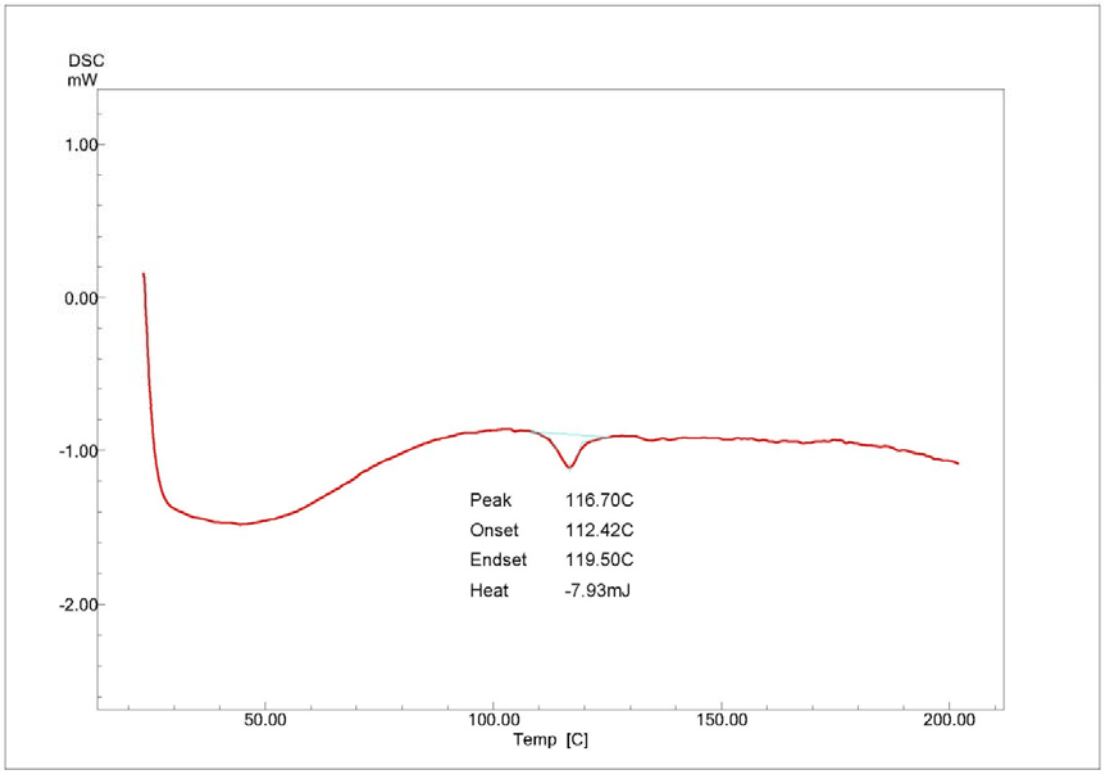


**Figure 3.3** DSC thermogram of spiramycin raw material.

**Thermal microscopy (TM)**

Micrographs of the raw material were taken to corroborate the $T_g$ event noted in the DSC thermogram. As described in the literature, the $T_g$ is often observed as the morphological change from a solid to a rounded liquid drop (Ymén, 2011). When the temperature region above $T_g$ (116.7ºC) is reached, the behaviour of the substance is accompanied by an increased molecular mobility. For this experiment a small amount of the sample was placed on a microscopic plate and covered with a cover slip, where after it was exposed to elevated temperatures as indicated in table 3.4.

**Table 3.4** Summary of TM results of spiramycin raw material

| 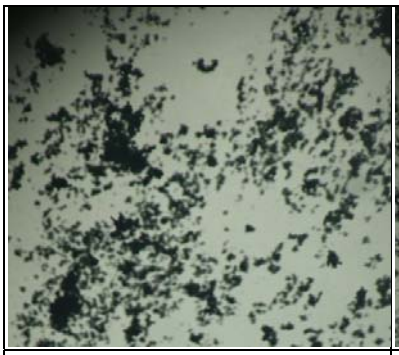 | 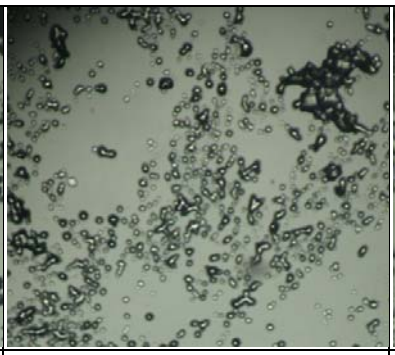 | 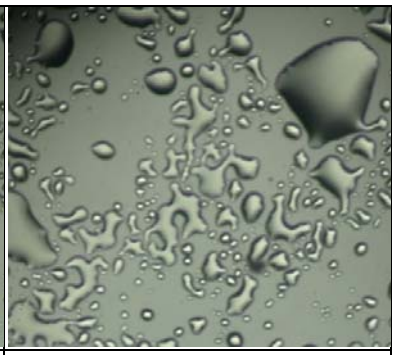 |
|---|---|---|
| Amorphous raw material at 22°C | Transition to the liquid form starting at 112°C | Fluid-like drops at 119°C |

**Scanning electron microscopy (SEM)**

In preparation, samples are fastened to a small piece of carbon tape, mounted onto a metal stub and coated with a gold-palladium film. The SEM photomicrographs in figure 3.4 clearly show the amorphous structure of the raw material, lacking the definitive morphological shape and well-defined crystal structure (Gilmore, 2011) one would observe for a crystalline substance at the same magnification. Another observation that can be made is the sponge-like surface of the spiramycin particles. This could lead to entrapment of solvents and water to a significant extent.

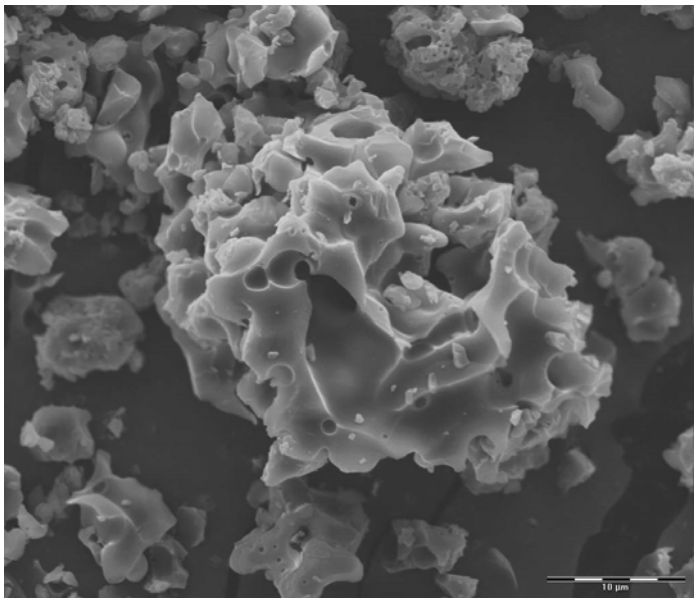

**Figure 3.4** The SEM micrograph of amorphous spiramycin raw material.

**X-ray powder diffraction (XRPD)**

The X-ray diffraction pattern of spiramycin raw material (figure 3.5) presented an amorphous "halo" pattern, and with the exception of the single peak found at 11.6, has no other detectable Bragg diffraction peaks. The lack of long-range order within the structure of spiramycin, a characteristic of all amorphous substances, causes this incoherent scattering of light (Bates *et al*., 2006).

**Table 3.5** Peak intensity ratios (I/Io) at main peak angles (°2θ) of spiramycin raw material.

| **Spiramycin raw material** | |
|---|---|
| **Peak angles °2θ** | **Intensities (I/Io)** |
| 11.6 | 100 |

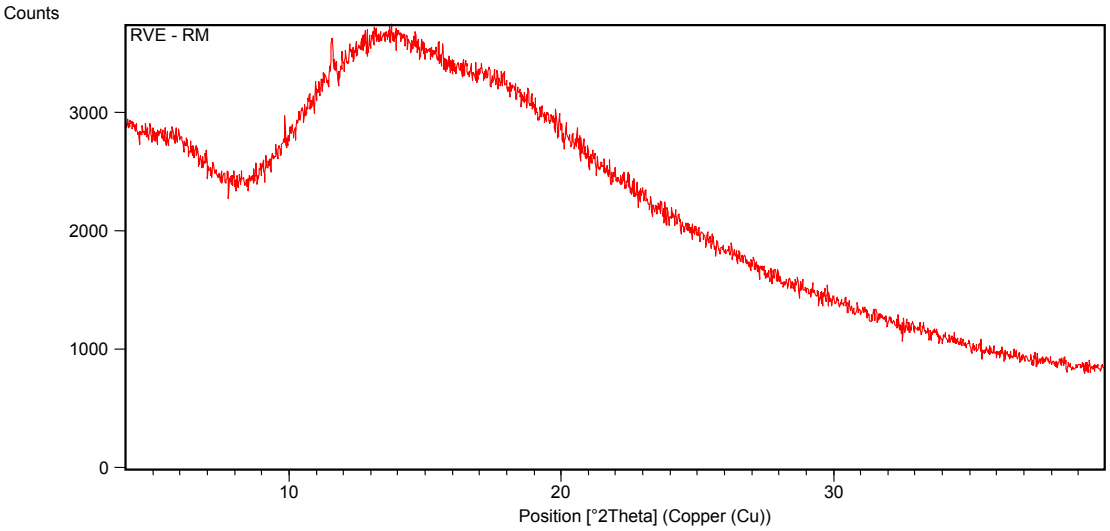


**Figure 3.5** The X-ray powder diffraction pattern of spiramycin raw material.

**Infrared spectroscopy (IR)**

Spiramycin samples were diluted with a non-absorbing KBr matrix in a 1-5% ratio (paragraph 2.6.1). DRIFTS were recorded as shown in figure 3.6 with main absorption peaks indicated in table 3.6, correlating well to those reported in the literature (Medicines Complete, 2010).

**Table 3.6** Main absorption peaks of spiramycin raw material with their corresponding wave numbers

| Main absorptions | Wavenumbers ($cm^{-1}$) |
|---|---|
| 1 | 567.1 |
| 2 | 869.9 |
| 3 | 904.6 |
| 4 | 993.3 |
| 5 | 1053.1 |
| 6 | 1161.2 |
| 7 | 1278.8 |
| 8 | 1722.4 |
| 9 | 3473.8 |

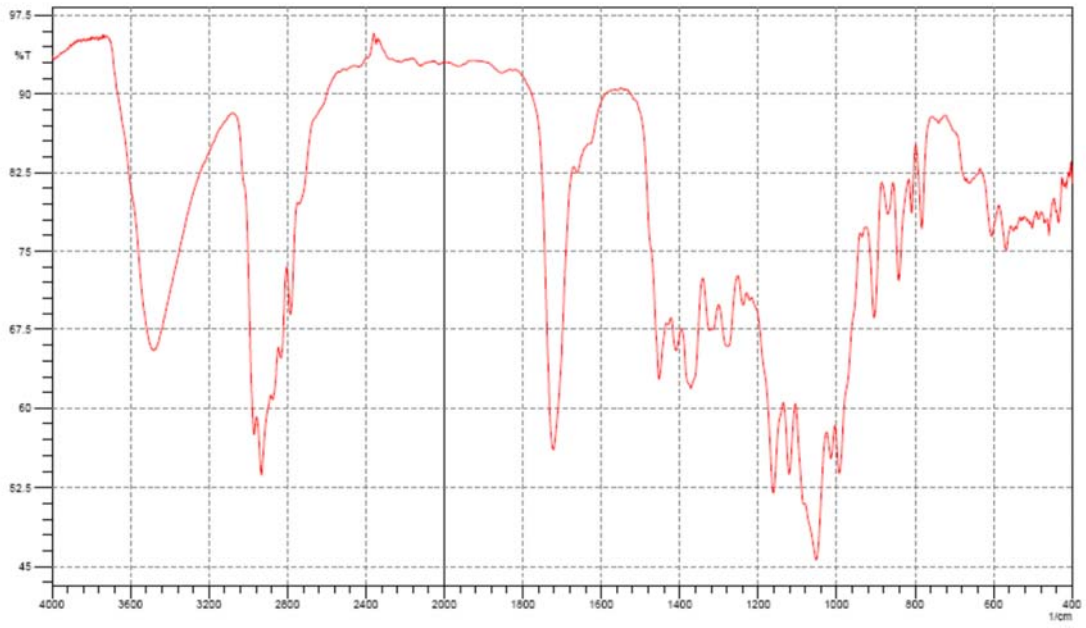


**Figure 3.6** The infrared spectrum of spiramycin raw material.

### 3.10.2 Recrystallisation from alcohols

The DSC traces of all the recrystallisation products were inconclusive and resulted in very complex thermograms. The DSC could therefore not be used as an identification or analytical technique to distinguish between the different recrystallisation products. In order to get the complete characterisation picture, the DSC thermogram of each recrystallisation product was, however included in the discussion.

#### 3.10.2.1 *n*-butanol

**Differential scanning calorimetry (DSC)**

DSC analysis was performed on samples weighing approximately 3-6 mg in pierced aluminium crimp cells. The samples were heated to a maximum temperature of 200ºC at a heating rate of 10ºC/min under a nitrogen purge flow of 35 ml/min. Figure 3.7 shows the DSC thermogram of spiramycin recrystallised from *n*-butanol. Multiple endothermic events were observed throughout the heating process. These events were associated with the effects of residual solvent release from the sample matrix. Following this, the sample started to degrade from the region of 140ºC. The residual solvent present in the sample as well as the effects of annealing, hampered the quantification of the $T_g$. The use of a modulated

DSC, which allows for separate viewing of these events, would have been useful as a characterisation technique.

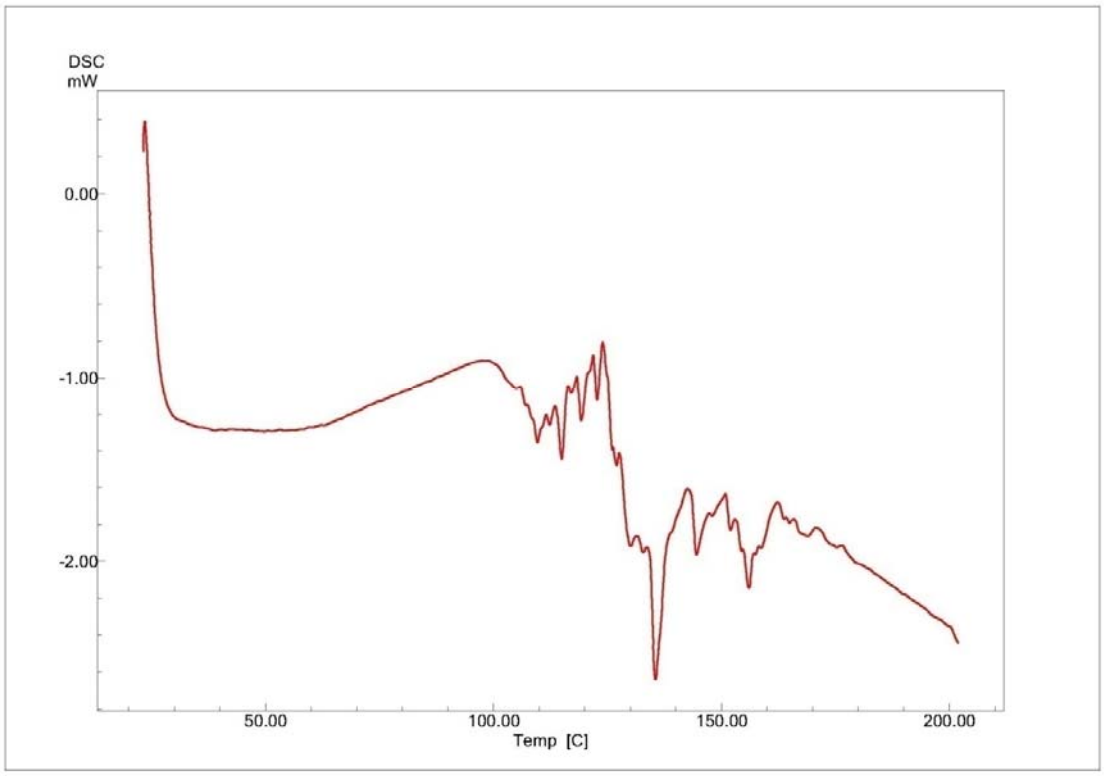


**Figure 3.7** DSC thermogram of amorphous spiramycin generated from *n*-butanol.

**Thermogravimetric analysis (TGA)**

The DSC results showed evidence of possible solvent inclusion/residual solvent within the structure of the sample. It was therefore decided to perform TGA. Theoretical weight loss was calculated to be 8.1% (for a 1:1 n-butanol solvate) compared to the experimental weight loss of 9.3%.

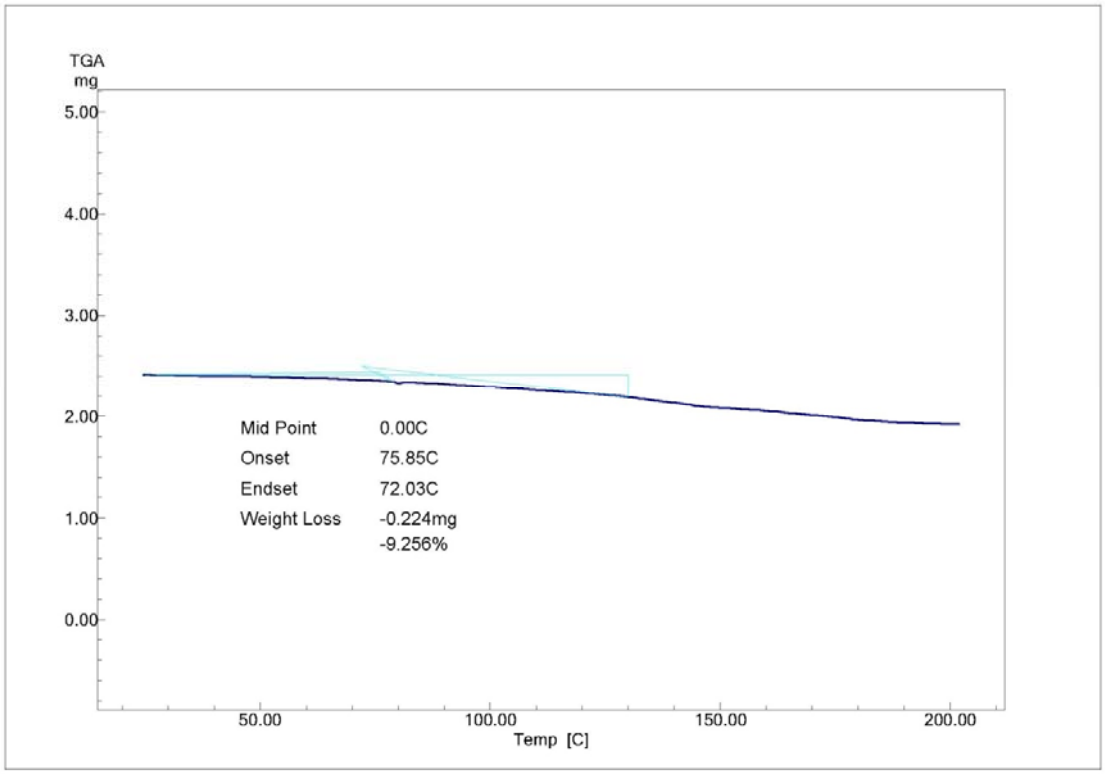


**Figure 3.8** The TGA of amorphous spiramycin generated from *n*-butanol.

**Thermal microscopy (TM)**

Table 3.7 shows TM photographs taken of samples immersed in silicone oil and subjected to the heat signal over the indicated temperature range.

**Table 3.7** TM results for amorphous samples generated from *n*-butanol

| | | |
|---|---|---|
|  | 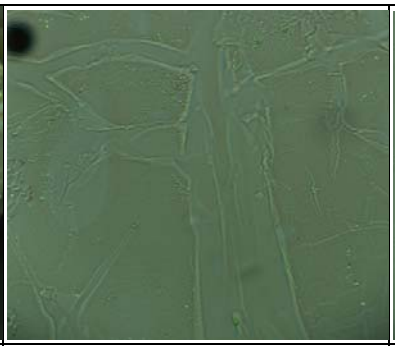 |  |
| Glass at 23ºC | Liquid formation at 111ºC | Liquid at 133ºC |

**Infrared spectroscopy (IR)**

Samples were diluted with a non-absorbing KBr matrix in a 1-5% ratio. DRIFTS were recorded as shown in figure 3.9 with main absorption peaks indicated in table 3.8. The main absorptions for samples recrystallised from *n*-butanol proved to be similar to those displayed by the raw material.

**Table 3.8** Main absorption peaks of spiramycin recrystallised from *n*-butanol

| Main absorptions | Wavenumbers ($cm^{-1}$) |
|---|---|
| 1 | 868.0 |
| 2 | 903.7 |
| 3 | 992.4 |
| 4 | 1053.1 |
| 5 | 1163.1 |
| 6 | 1273.1 |
| 7 | 1725.4 |

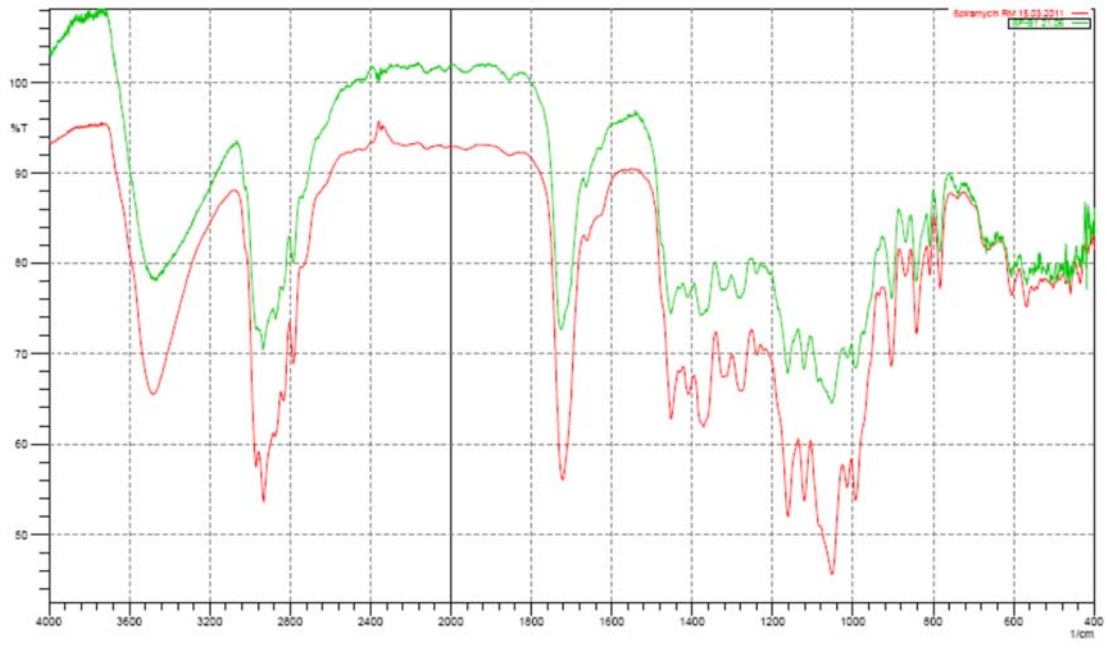


**Figure 3.9** Overlay of the infrared spectrum of spiramycin recrystallised from *n*-butanol (green) and the raw material (red).

#### 3.10.2.2 2-butanol

The product obtained through recrystallisation from 2-butanol was an adhesive, viscous mass, showing no morphological signs of crystallinity. This type of consistency was present with the majority of the tested samples. What made the analysis of these materials difficult was to ensure that the samples were blotted sufficiently dry, to prevent surface moisture/solvent distorting the thermal behaviour of these systems. The perplexity of the DSC thermograms is evident throughout this chapter.

**Differential scanning calorimetry (DSC)**

DSC analysis was performed on spiramycin recrystallised from 2-butanol. The method described in paragraph 2.2.1 was used. In figure 3.10, numerous exothermic and endothermic events are observed between 100ºC and 150ºC, followed by what appears to be sample degradation. Considering the SEM micrograph depicted in figure 3.4, it could be postulated that the holes or gaps visible on the surface of the powder could trap solvent. This will explain the multiple thermal events visible on the DSC thermogram.

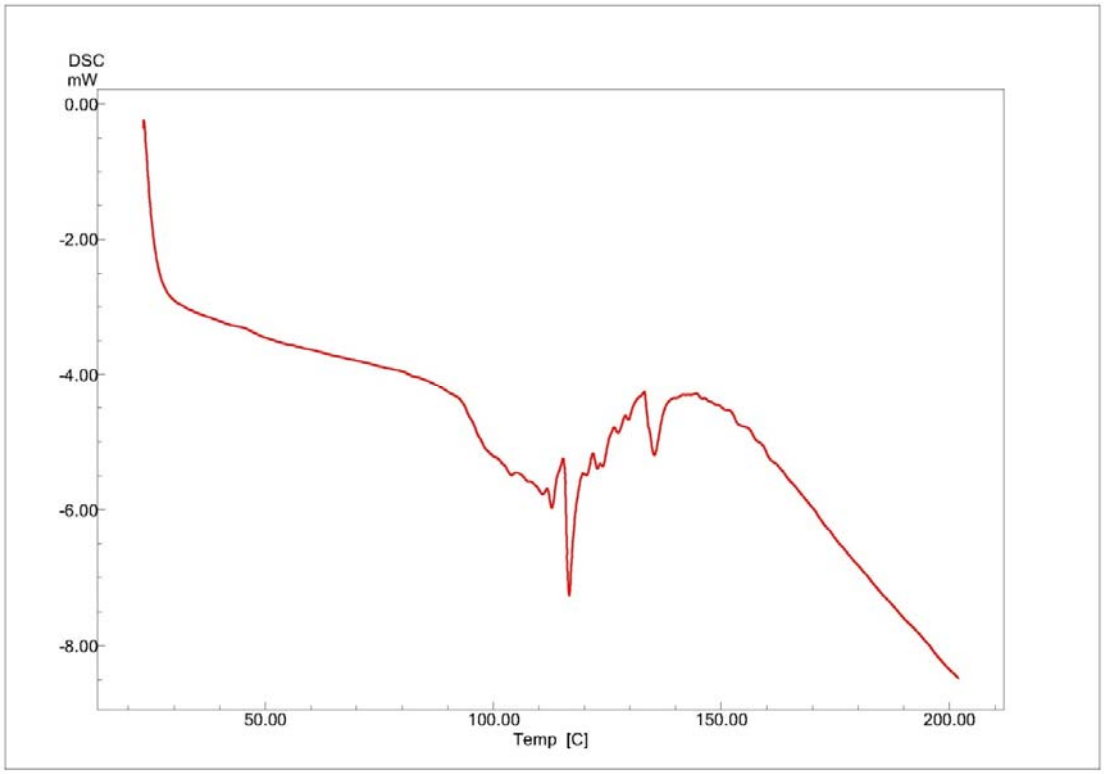


**Figure 3.10** DSC thermogram of spiramycin recrystallised from 2-butanol.

**Thermogravimetric analysis (TGA)**

The TGA thermogram for samples generated from 2-butanol (figure 3.11) shows the experimental weight loss of 18.1%. Since crystalline materials pack closely together to maximise molecular interaction, they have little extra space for solvent uptake, therefore the amount of solvent present usually does not exceed 0.5%. However, according to Griesser (2006), localised disordered areas or amorphicity are regarded as the most common reason for increased residual solvent contents. The metastable areas are able to host large amounts of solvent that can more or less “dissolve” in these highly energetic areas. Since the XRPD pattern clearly shows the amorphous nature of the sample (figure 3.4), it could explain the high experimental weight (18.0 %) loss in comparison with its theoretical weight loss.

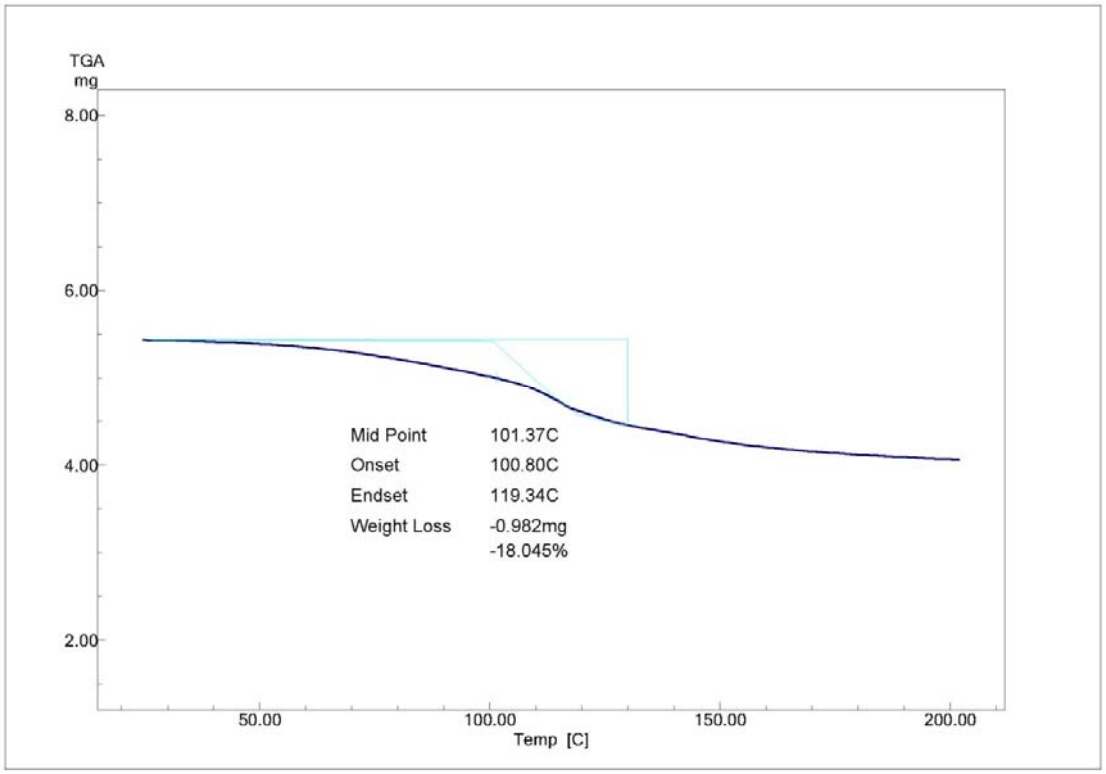


**Figure 3.11** The TGA of amorphous spiramycin recrystallised from 2-butanol.

**Thermal microscopy (TM)**

Table 3.9 shows the morphological changes from the amorphous solid to a fluid recorded over the given temperature range. The darker spots on the photos were presumably entrapped solvent within the sample matrix which evaporated at approximately the temperature where the weight loss commenced on the TGA thermogram in figure 3.11. The transition to the liquid form ($T_g$) at 115ºC was similar to what was observed in the raw material.

**Table 3.9** TM results for spiramycin recrystallised from 2-butanol

| | |
|---|---|
|  |  |
| Amorphous spiramycin at 23°C | Transition to the liquid form at 115ºC |

**Infrared spectroscopy (IR)**

DRIFTS were recorded as shown in figure 3.12 with main absoption peaks indicated in table 3.10. The infrared spectrum of spiramycin recrystallised from 2-butanol corresponded well in some areas to the spectrum of the raw material, but differed for instance at 2358.1 $cm^{-1}$ and 2342.7 $cm^{-1}$. Since this recrystallisation product probably contains residual solvent (TGA results), the infrared spectrum should differ from the raw material.

**Table 3.10** Main absorption peaks of spiramycin recrystallised from 2-butanol.

| Main absorptions | Wavenumbers ($cm^{-1}$) |
|---|---|
| 1 | 563.2 |
| 2 | 869.9 |
| 3 | 900.8 |
| 4 | 989.5 |
| 5 | 1052.2 |
| 6 | 1161.2 |
| 7 | 1275.0 |
| 8 | 1722.4 |
| 9 | 2342.7 |

**Table 3.10** (continued)

| Main absorptions | Wavenumbers ($cm^{-1}$) |
|---|---|
| 10 | 2358.1 |
| 11 | 3473.8 |

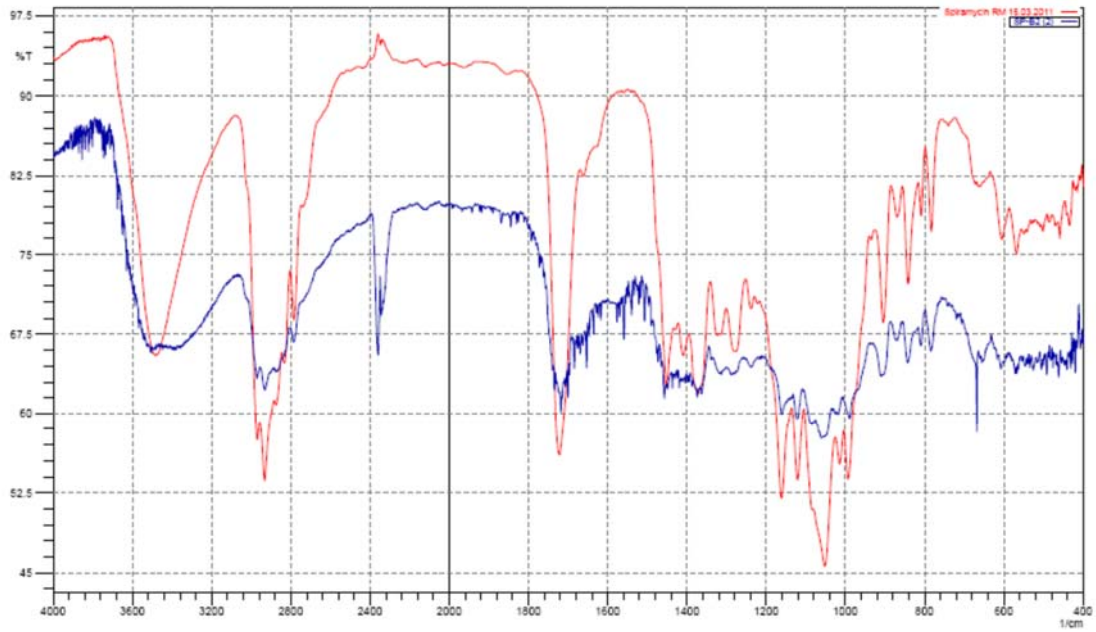


**Figure 3.12** Overlay of the infrared spectrum of spiramycin recrystallised from 2-butanol (blue) and the raw material (red).

### 3.10.2.3 Ethanol (EtOH)

Recrystallisation products from ethanol and methanol both produced amorphous materials described in section 3.9. As with the majority of the samples that were analysed, the intricate nature of these samples greatly influenced the interpretability of the DSC thermograms.

**Differential scanning calorimetry (DSC)**

The DSC thermogram depicts a multitude of thermal events. Once again the high percentage weight loss and the multiple thermal events observed could be due to the entrapment of solvent into the gaps of the spiramycin particles. The temperatures of the first

endothermic events correlate well with the boiling point of ethanol (≅78°C), suggesting the evaporation of ethanol upon heating. The thermal events after 100°C subsequently signify the $T_g$ of spiramycin as well as further evaporation of ethanol from the irregular particles.

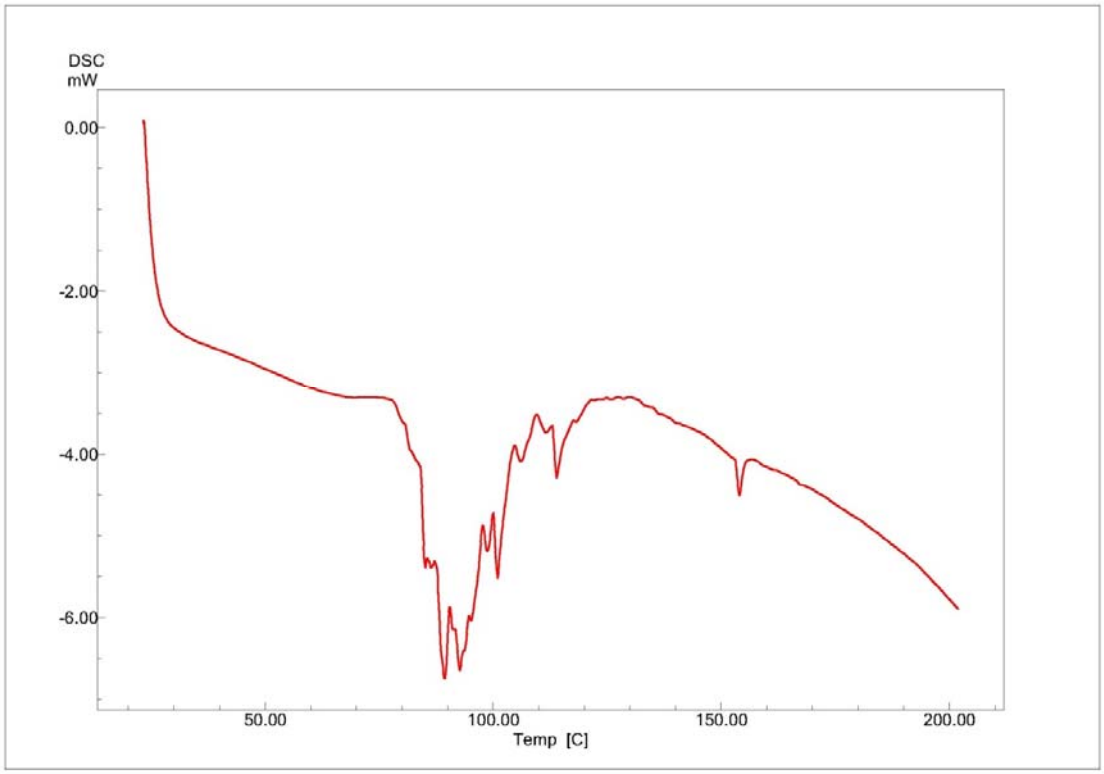


**Figure 3.13** DSC thermogram of spiramycin recrystallised from EtOH.

**Thermogravimetric analysis (TGA)**

The differential thermal gravimetry thermogram (DTG) is shown in figure 3.14, indicating a weight loss of 14.8%. The theoretical weight loss due to desolvation is 5.2% for 1:1 spiramycin:ethanol solvate. The experimental value would normally be indicative of a 1:3 spiramycin:ethanol solvate in a crystalline material. The start of the weight loss on the TGA thermogram (blue) coincides with what is believed to be the evaporation of ethanol from the sample in the form of a broad endotherm on the DSC (red), starting at approximately 90ºC.

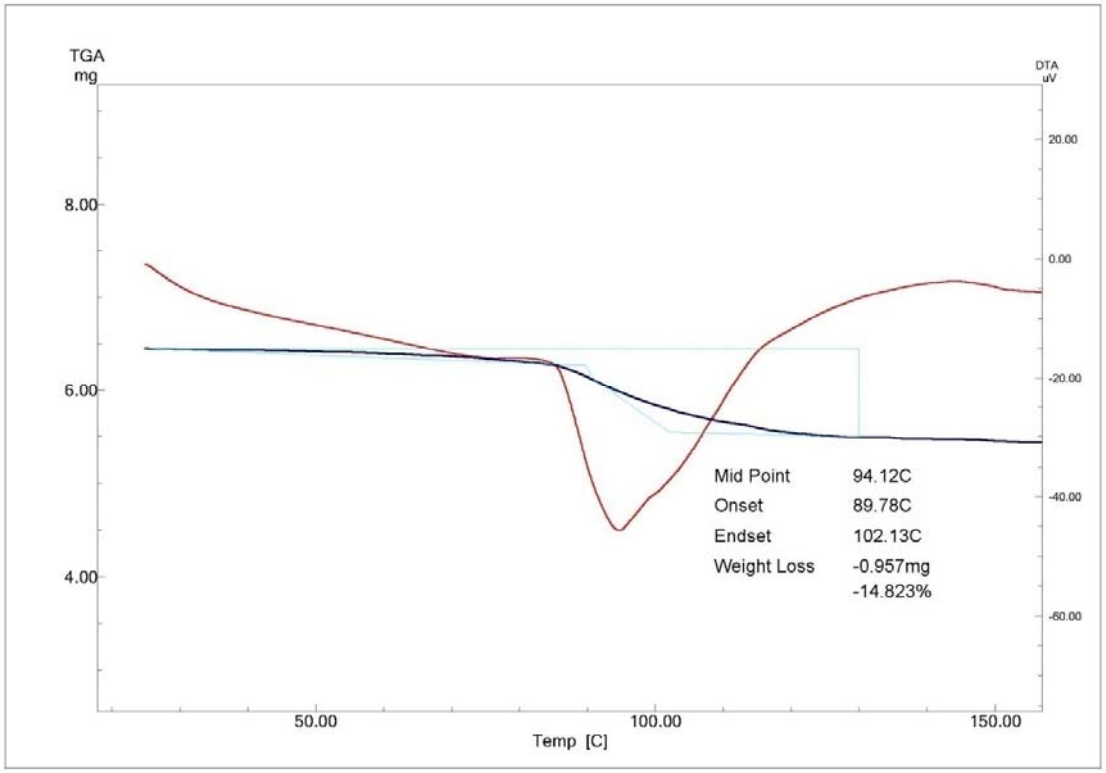


**Figure 3.14** The DTG of spiramycin recrystallised from EtOH.

**Thermal microscopy (TM)**

Micrographs captured by means of thermal microscopy are displayed in table 3.11.

**Table 3.11** TM results for spiramycin recrystallised from EtOH.

| | | |
|---|---|---|
|  |  | 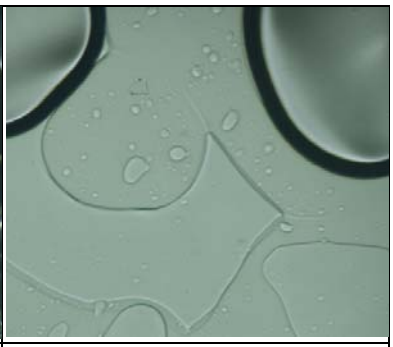 |
| Amorphous spiramycin at 23°C | Gas evolution at approximately 85ºC | Liquid at 110°C |

**Infrared spectroscopy (IR)**

DRIFTS were recorded as shown in figure 3.15 with main absorption peaks indicated in table 3.12. The main absorptions for spiramycin recrystallised from ethanol were similar to those displayed by the raw material.

**Table 3.12** Main absorption peaks of spiramycin recrystallised from EtOH.

| Main absorptions | Wavenumbers ($cm^{-1}$) |
|---|---|
| 1 | 567.1 |
| 2 | 869.9 |
| 3 | 904.6 |
| 4 | 993.3 |
| 5 | 1053.1 |
| 6 | 1161.2 |
| 7 | 1284.6 |
| 8 | 1714.7 |
| 9 | 3475.3 |

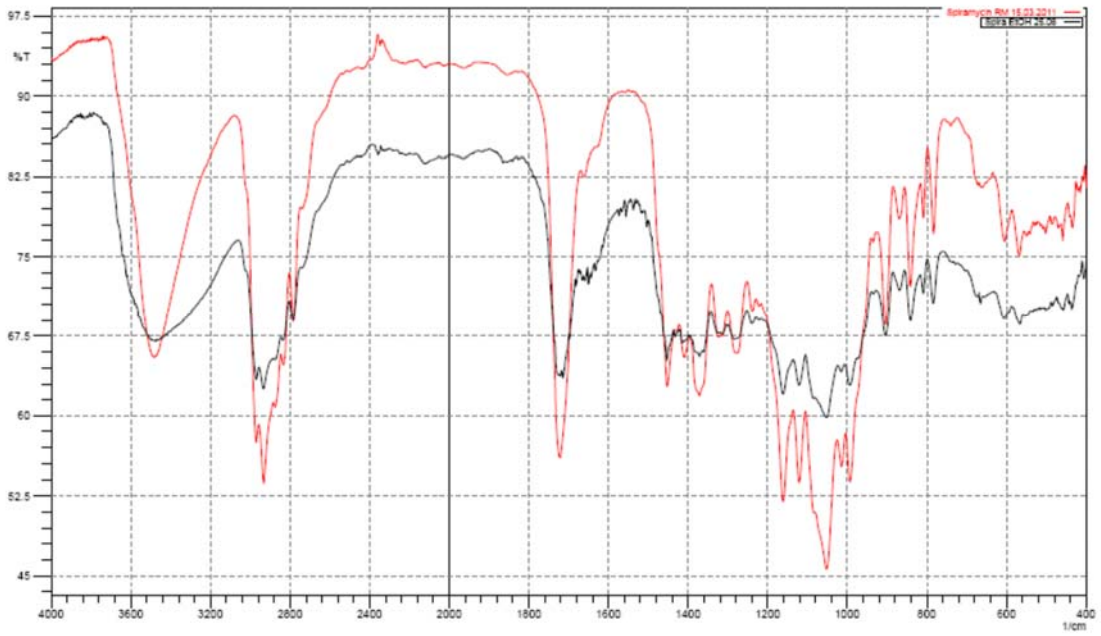


**Figure 3.15** Overlay of the infrared spectrum of spiramycin recrystallised from EtOH (black) and the raw material (red).

### 3.10.2.4 Methanol (MeOH)

**Differential scanning calorimetry (DSC)**

DSC results illustrated in figure 3.16 display a narrow sharp endotherm at 78.6ºC, presumably due to solvent evaporation from the surface of the sample. It is possible that some methanol was engulfed by the amorphous sample matrix. However once the $T_{g.}$ was reached, methanol present within the sample started to evaporate at 100ºC as seen on the DSC thermogram.

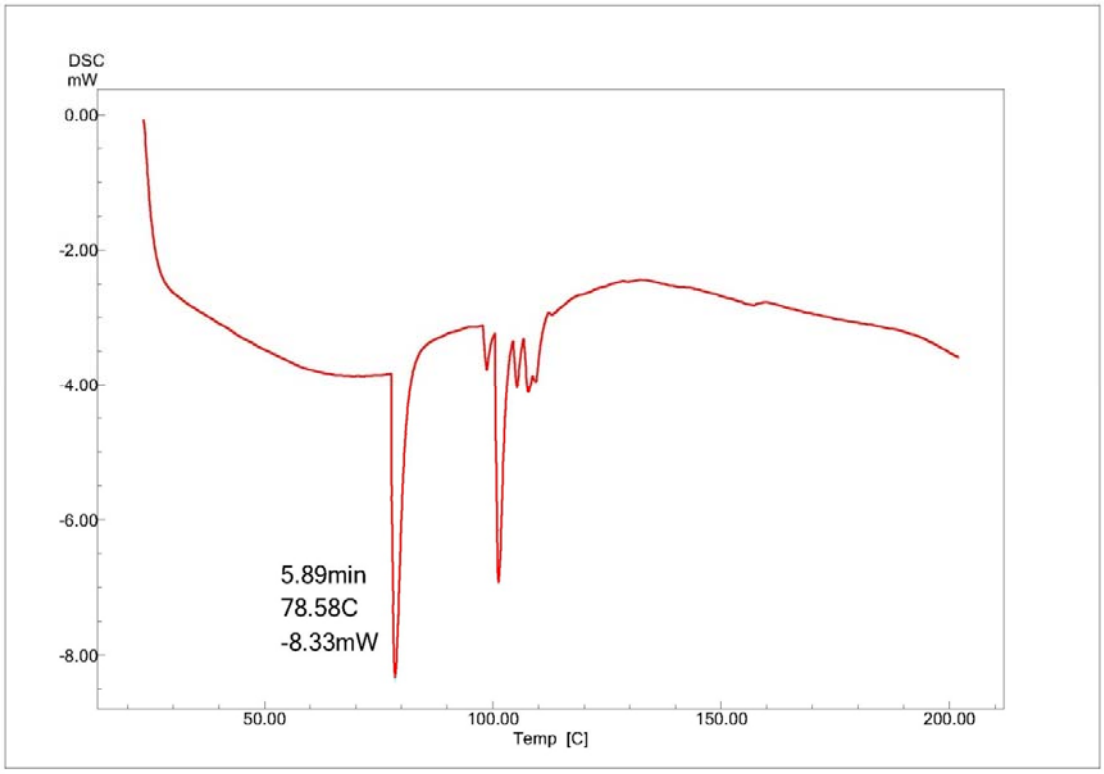


**Figure 3.16** DSC thermogram of spiramycin recrystallised from methanol.

**Thermogravimetric analysis (TGA)**

Experimental weight loss according to the results (figure 3.17) is 14.6%., compared to the theoretical weight loss of 3.7% for solvate formation. The weight loss starting at 70.8ºC on the TGA thermogram (blue), yet again pointed to the evaporation of methanol from the sample as it coincides with the start of a broad endotherm on the DSC thermogram (red).

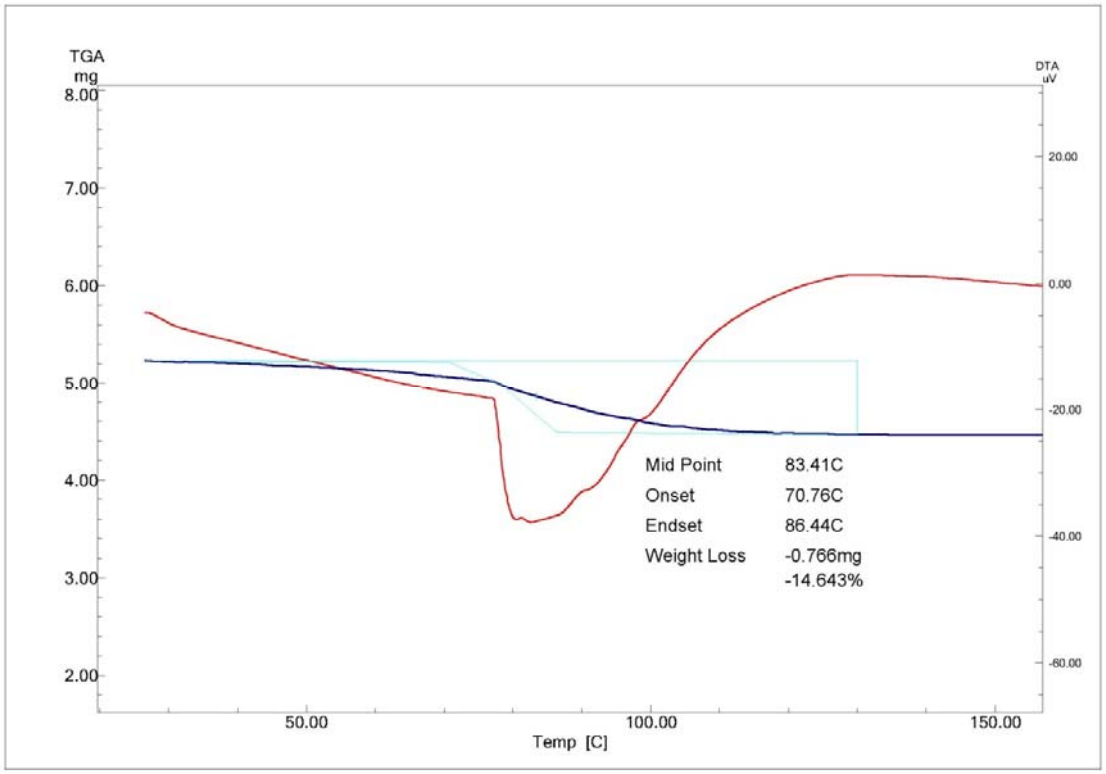


**Figure 3.17** The DTG of spiramycin recrystallised from MeOH.

**Thermal microscopy (TM)**

Gas evolution was evident throughout the heating process as displayed by the TM photomicrographs. This could partly be due to air bubbles present in the silicone oil.

**Table 3.13** TM results for spiramycin recrystallised from MeOH

| | | |
|---|---|---|
| 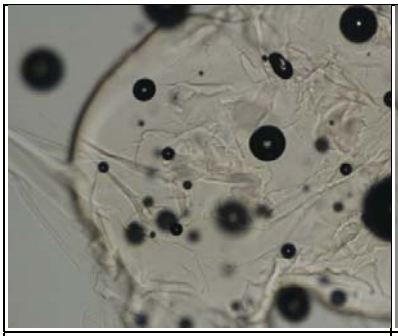 |  | 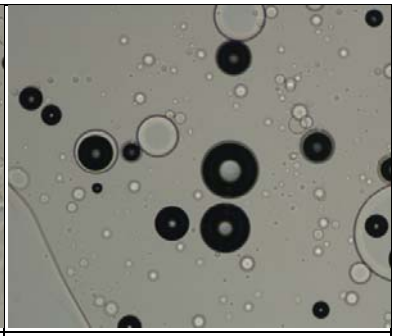 |
| Amorphous spiramycin at 21°C | Transition to the liquid form at 82ºC | Liquid at 94°C |

**Infrared spectroscopy (IR)**

DRIFTS were recorded as shown in figure 3.18 with main absorption peaks indicated in table 3.14. The IR overlay shows that the spectra of the MeOH recrystallisation product and that of the raw material were almost identical. Small differences were however visible; the peaks observed at 2339.7 $cm^{-1}$ and 2358.9 $cm^{-1}$ were not present in the IR spectrum of the raw material.

**Table 3.14** Main absorption peaks of spiramycin recrystallised from MeOH

| Main absorptions | Wavenumbers ($cm^{-1}$) |
|---|---|
| 1 | 567.1 |
| 2 | 869.9 |
| 3 | 904.6 |
| 4 | 993.3 |
| 5 | 1053.1 |
| 6 | 1161.2 |
| 7 | 1278.8 |
| 8 | 1714.7 |
| 9 | 2339.7 |
| 10 | 2358.9 |
| 11 | 3468.0 |

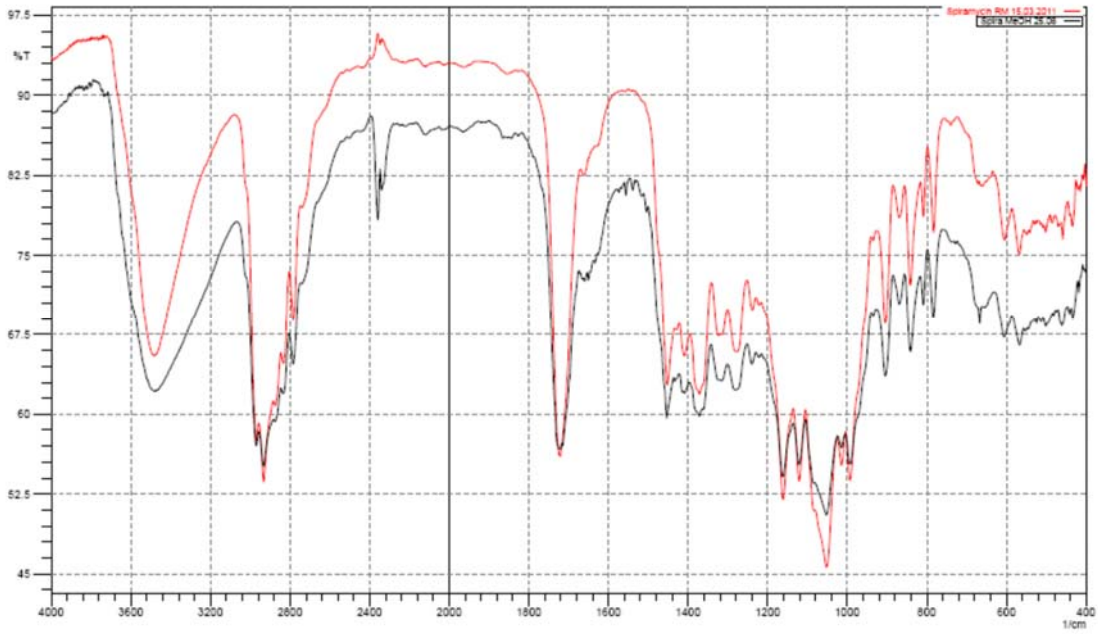


**Figure 3.18** Overlay of the infrared spectrum of spiramycin recrystallised from MeOH (black) and the raw material (red).

### 3.10.2.5 1-propanol

**Differential scanning calorimetry (DSC)**

Once again a complex DSC trace was obtained. The DSC trace obtained from the recrystallisation product from 1-propanol was similar to that of the previous discussed thermograms. No definite $T_g$ could be identified and DSC as a technique seemed not adequate as analytical tool for spiramycin.

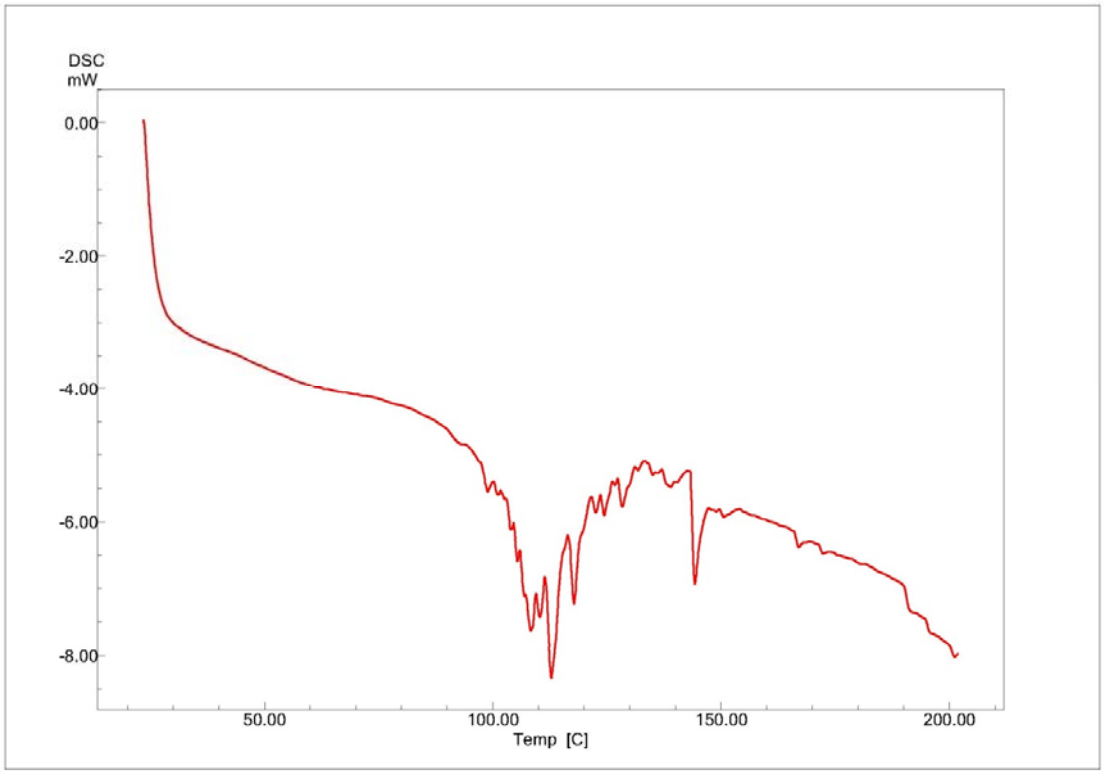


**Figure 3.19** DSC thermogram of spiramycin recrystallised from 1-propanol.

**Thermogravimetric analysis (TGA)**

Theoretical weight loss of 6.7% (for a 1:1 spiramycin: 1-propanol solvate) is much lower than what was experimentally achieved (15.0%).

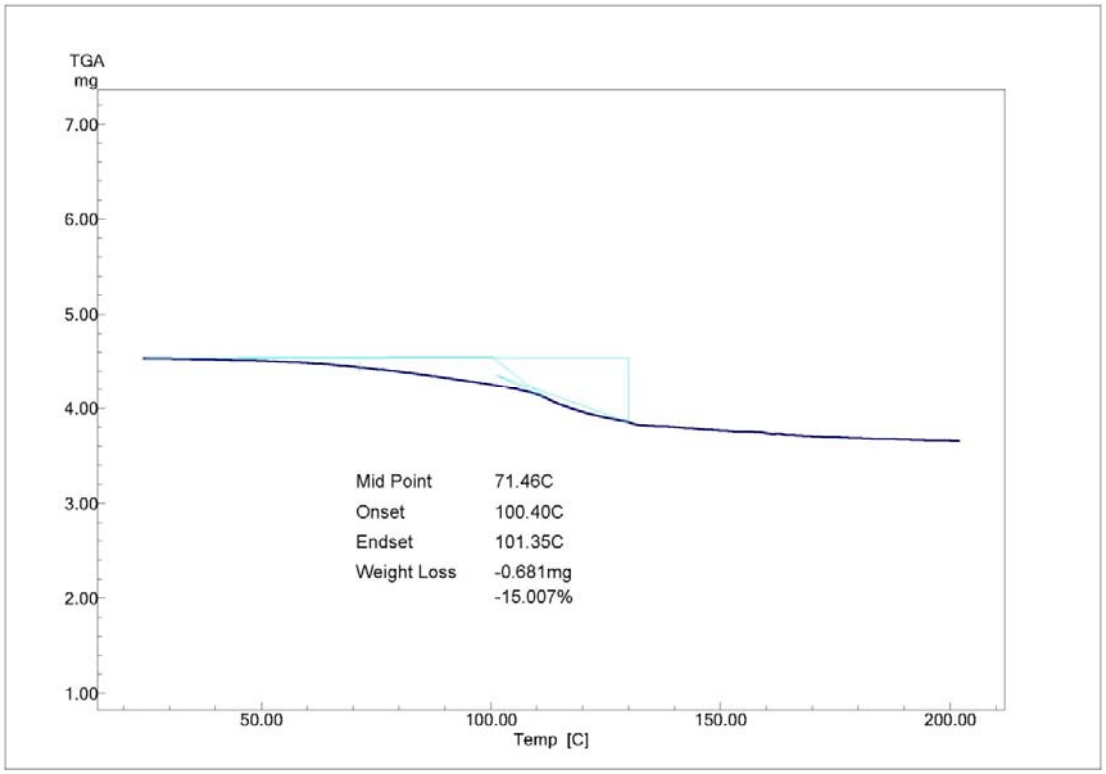


**Figure 3.20** The TGA of spiramycin recrystallised from 1-propanol.

**Thermal microscopy (TM)**

The transition to the liquid form is significantly lower in comparison with all the above-mentioned products. No clear $T_g$ could be identified from the DSC results. The TG results showed a significant percentage of weight loss, most probably due to a large amount of 1-propanol entrapped between and within the sponge-like particles. From the micrographs depicted in table 3.15, it could be concluded that the amount of 1-propanol present in the sample is so high that upon heating and release of solvent from the particles, spiramycin actually starts to dissolve in the released 1-propanol. This would explain the multitude of thermal events evident on the DSC thermogram.

**Table 3.15** TM results for spiramycin recrystallised from 1-propanol

| | | |
|---|---|---|
|  |  | 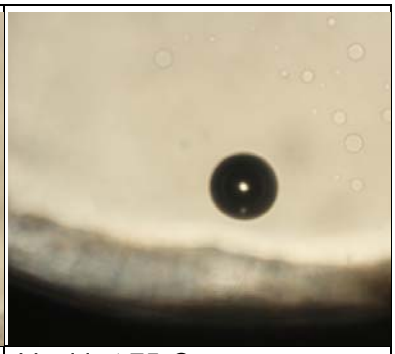 |
| Amorphous spiramycin at 21°C | Transition to the liquid form from 72°C | Liquid at 75°C |

**Infrared spectroscopy (IR)**

DRIFTS were recorded as shown in figure 3.21 with main absorption peaks indicated in table 3.16. The main absorptions for spiramycin recrystallised from 1-propanol were similar to that of the raw material.

**Table 3.16** Main absorption peaks of spiramycin recrystallised from 1-propanol.

| Main absorptions | Wavenumbers ($cm^{-1}$) |
|---|---|
| 1 | 567.1 |
| 2 | 869.9 |
| 3 | 903.7 |
| 4 | 994.4 |
| 5 | 1051.3 |
| 6 | 1163.2 |
| 7 | 1273.1 |
| 8 | 1725.4 |

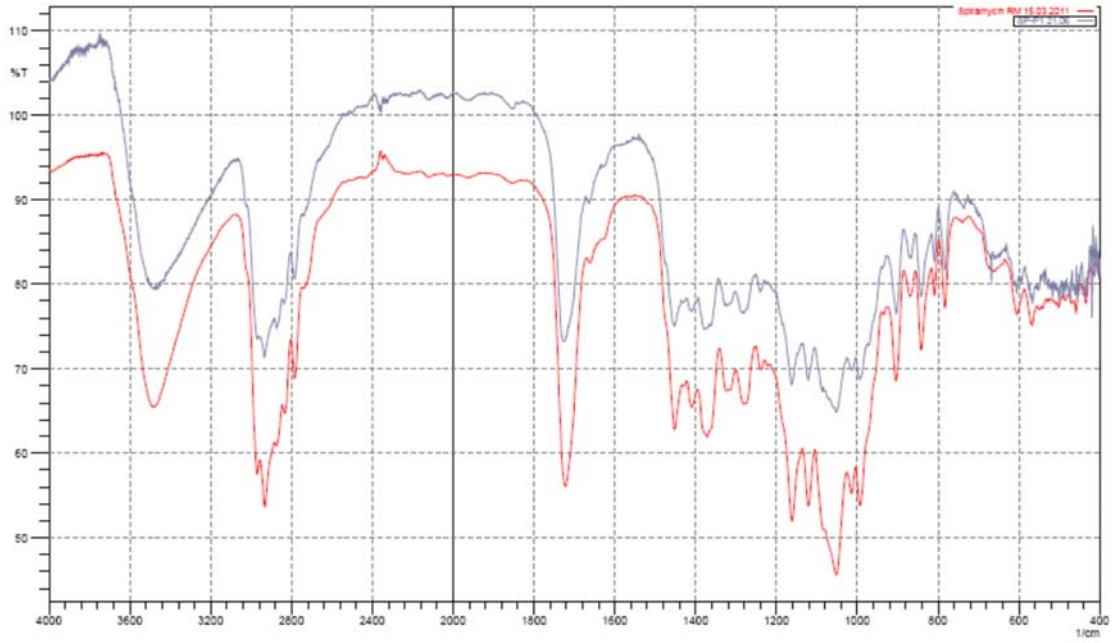


**Figure 3.21** Overlay of the infrared spectrum of spiramycin recrystallised from 1-propanol (blue) and the raw material (red).

### 3.10.2.6 Iso-propanol

**Differential scanning calorimetry (DSC)**

The DSC trace from iso-propanol is a broad endotherm at about 100°C and it differed from that of the other recrystallisation products.

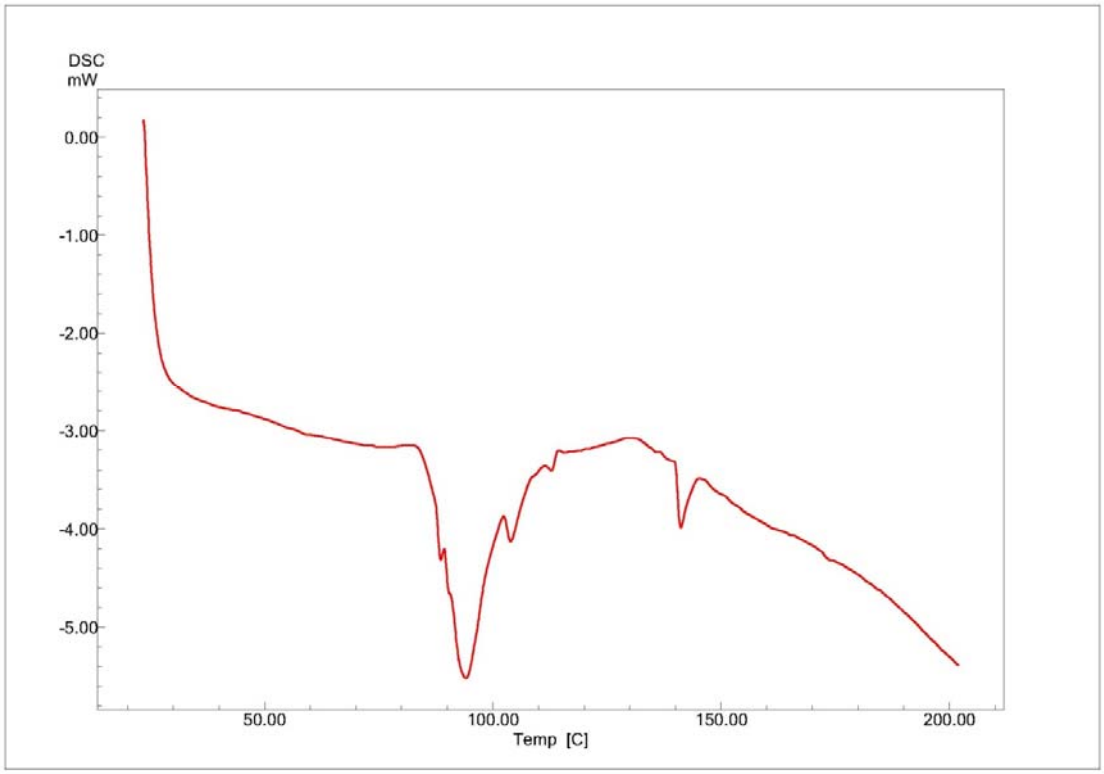


**Figure 3.22** DSC thermograms of spiramycin recrystallised from iso-propanol.

**Thermogravimetric analysis (TGA)**

Theoretical weight loss due to desolvation of a 1:1 iso-propanol:spiramycin solvate is 6.7%. The results generated experimentally were more than double than expected for a 1:1 solvate, with a weight loss of 14.6%.

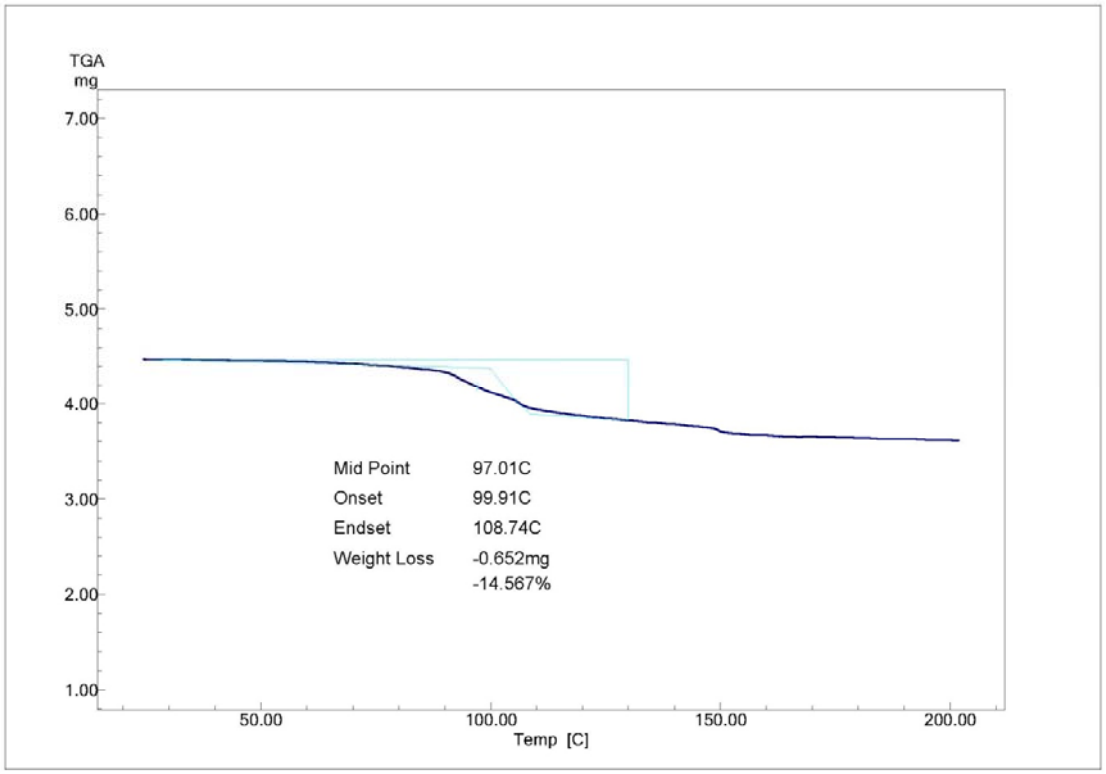


**Figure 3.23** The TGA of spiramycin recrystallised from iso-propanol.

**Thermal microscopy (TM)**

Table 3.17 is a summary of the TM photographs taken throughout the heating process on the hot-stage microscope.

**Table 3.17** TM results for spiramycin recrystallised from iso-propanol

| | | |
|---|---|---|
| 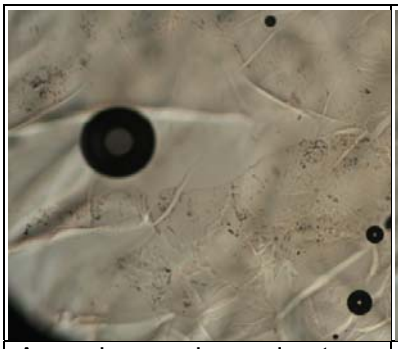 |  | 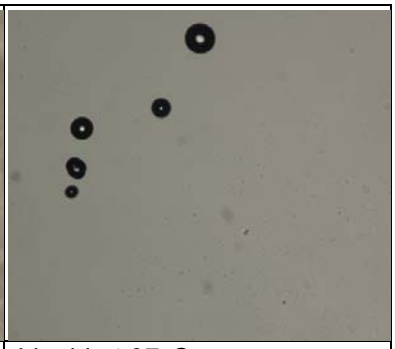 |
| Amorphous spiramycin at 27°C | Conversion to the liquid phase starting at 74°C | Liquid at 97°C |

**Infrared spectrum (IR)**

DRIFTS were recorded as shown in figure 3.23 with main absorption peaks indicated in table 3.18.

The main absorptions for spiramycin recrystallised from iso-propanol compared well with the raw material. The DTG showed the possibility of an iso-propanol solvate, but with the identical IR spectra, that is ruled out.

**Table 3.18** Main absorption peaks of spiramycin recrystallised from iso-propanol.

| Main absorptions | Wavenumbers ($cm^{-1}$) |
|---|---|
| 1 | 564.2 |
| 2 | 869.0 |
| 3 | 903.7 |
| 4 | 994.4 |
| 5 | 1160.2 |
| 6 | 1278.9 |
| 7 | 1724.4 |
| 8 | 3468.2 |

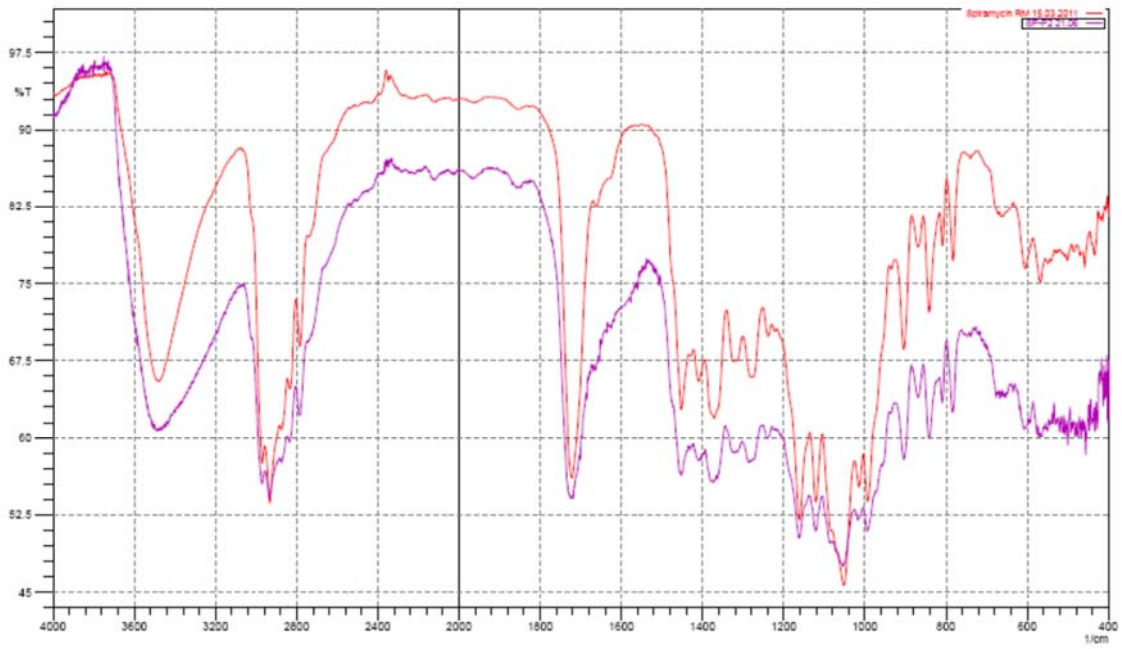


**Figure 3.24** Overlay of the infrared spectrum of spiramycin recrystallised from iso-propanol (purple) and the raw material (red).

### 3.10.2.7 Discussion of the data generated from alcohol solvents

It was evident from the data generated from thermal analysis, that there are significant inter-sample variations. Amorphous substances lack the abrupt discontinuity in enthalphy, volume and entropy that occurs as a result of first order phase transitions such as melting and vaporisation. Instead the step change in the baseline associated with the $T_g$ is usually the defining characteristic for an amorphous substance like spiramycin (Zhang & Zhou, 2009). Since most of the compounds were binary mixtures comprising the raw material and the liquid solvent, this event was difficult to observe on the DSC (figure 3.27). Thermal events associated with the physical aging of the substance could also have played a role. The characterisation of these samples was therefore more reliant on spectroscopic and crystallographic methods, which proved to be more useful in this instance since the results were reproducible, and therefore comparable. Forms generated from *n*-butanol, ethanol, 1-propanol and iso-propanol were comparable to that of the raw material. Forms generated from 2-butanol and methanol showed characteristic peaks in the region of 2000-2400 $cm^{-1}$, that were not present in the raw material (figure 3.25). There are, however, no significant differences between any of these solvents when their X-ray patterns are compared (figure 3.26).

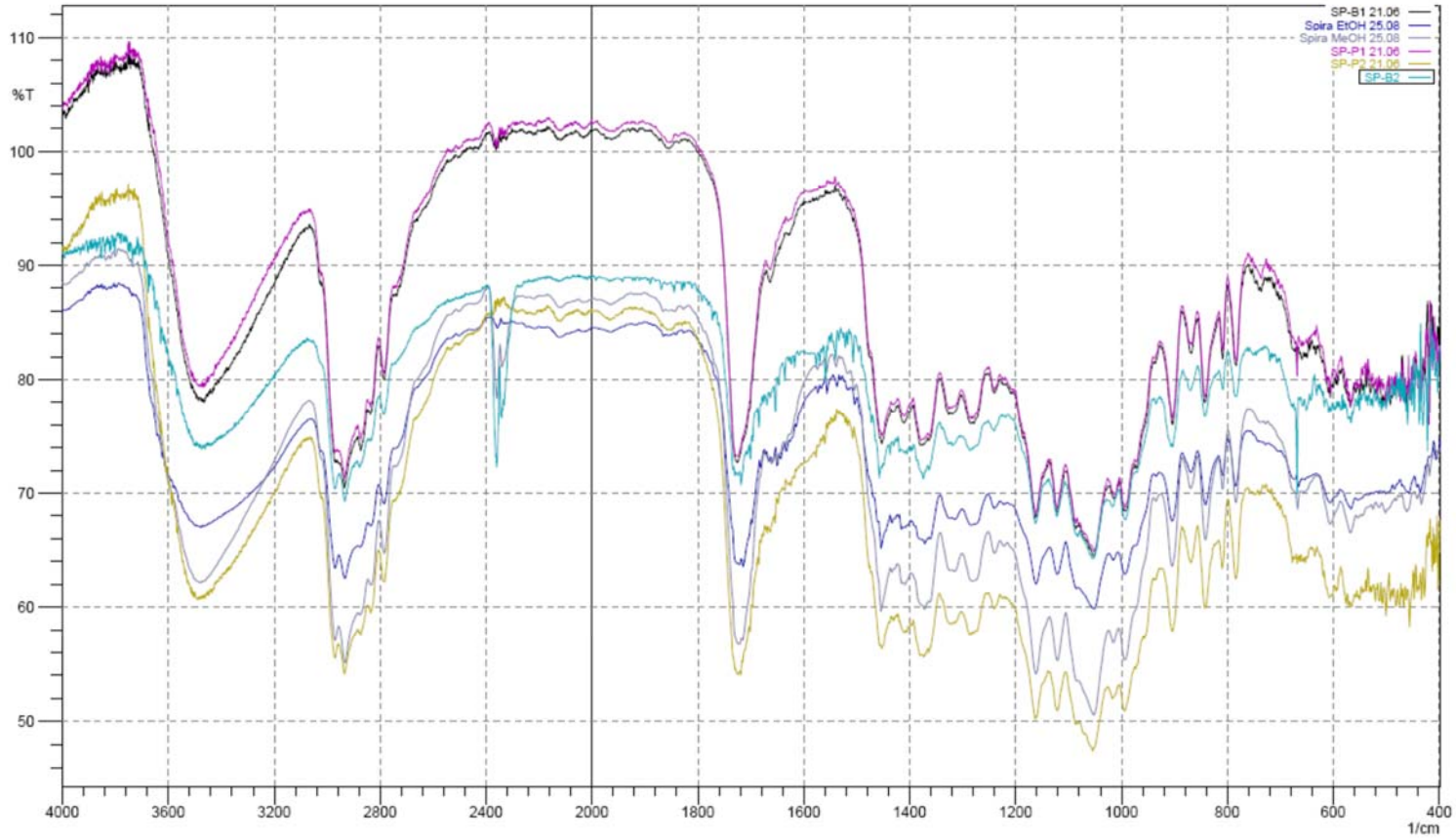


**Figure 3.25** Overlay of the IR spectra of the different amorphous forms generated from the alcohol group.

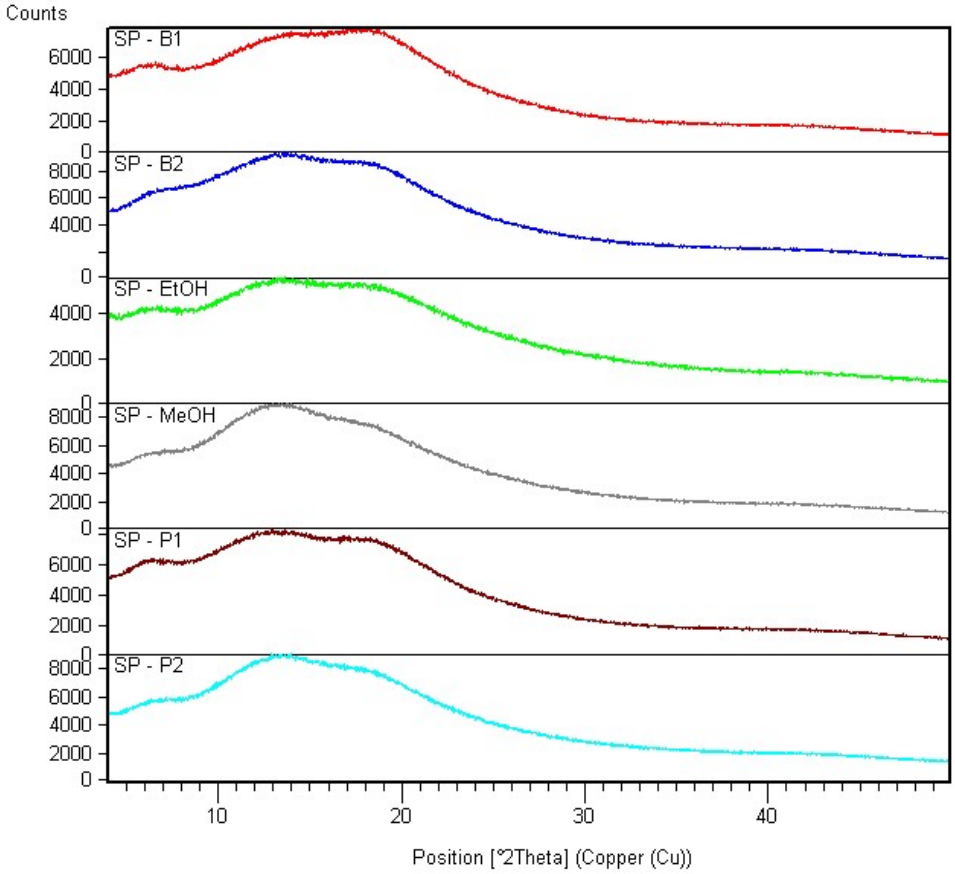


**Figure 3.26** Stack graph showing the amorphous XRPD patterns for samples generated from the alcohol group.

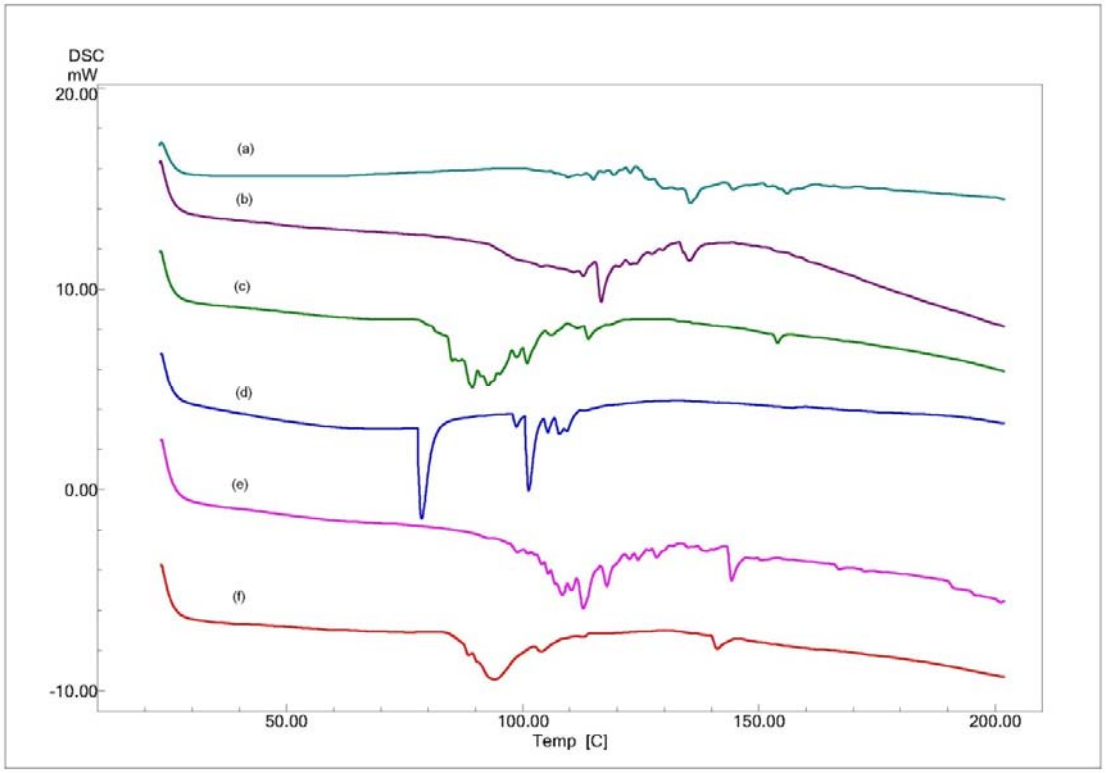


**Figure 3.27** DSC thermograms of the recrystallisation products from the alcohol group showing the complexity of this analytical method: (a) *n*-butanol (b) 2-butanol (c) ethanol (d) methanol (e) 1-propanol (f) iso-propanol.

### 3.10.3 Recrystallisation from diverse solvents

#### 3.10.3.1 Acetone

**Differential Scanning Calorimetry (DSC)**

Figure 3.28 shows the DSC thermogram of spiramycin recrystallised from acetone. As was the case with the alcohols, numerous thermal events were observed in the thermogram which made it difficult to pinpoint the exact temperature of $T_g$. The TM results were not very informative in this regard either. The sharp endothermic peak could indicate the evaporation of recrystallising solvent from the sample matrix.

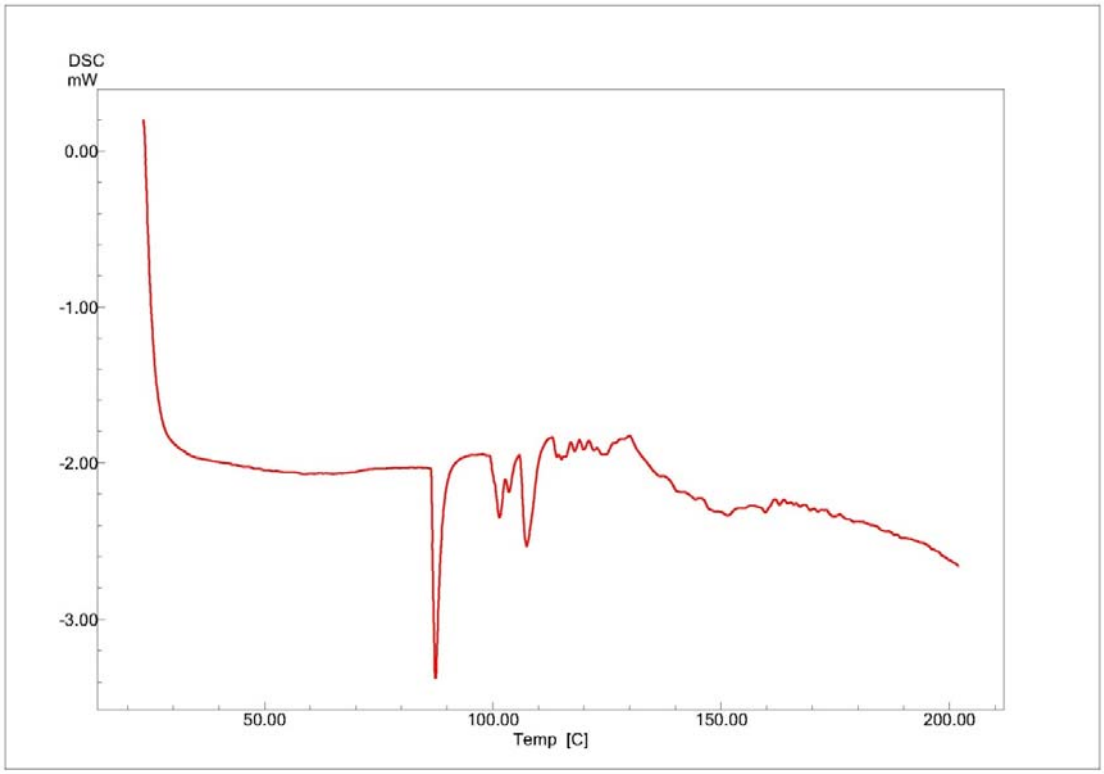


**Figure 3.28** The DSC thermogram of spiramycin recrystallised from acetone.

**Thermogravimetric analysis (TGA)**

The experimental weight loss for 1:1 spiramycin: acetone solvate was measured to be 13.8%, which exceeds the theoretical weight loss of 6.4% because of the amorphous nature of the sample (figure 3.29). This could normally be indicative of a 2:1 acetone:spiramycin solvate.

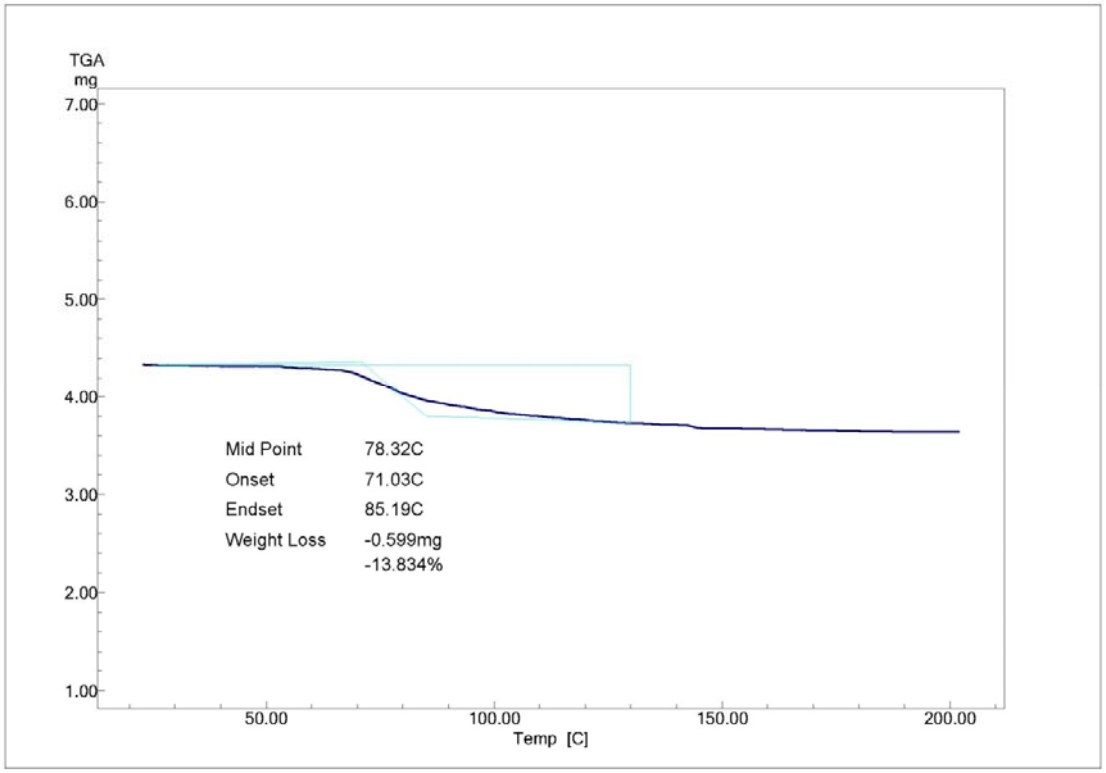


**Figure 3.29** The TGA of amorphous spiramycin recrystallised from acetone.

**Thermal microscopy (TM)**

Samples recrystallised from acetone was placed on a microscope glass plate, immersed in silicone oil and covered with a cover plate. TM results in table 3.19 show the pictures taken of samples over the elevated temperature range. It is evident from the TM pictures that solvent is indeed released from the sample. Bubble formation in the silicone oil is usually indicative of solvent release from the sample matrix.

**Table 3.19** TM results of spiramycin recrystallised from acetone

| | | |
|---|---|---|
| 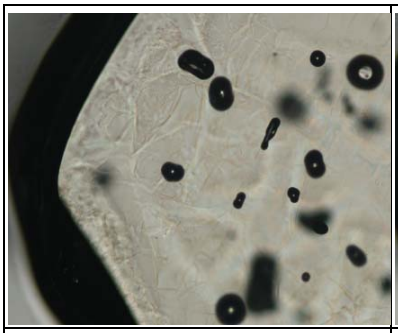 | 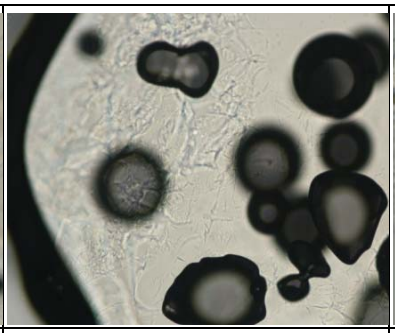 | 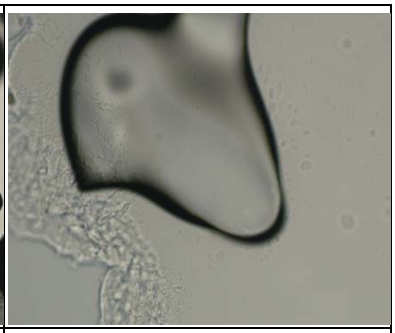 |
| Amorphous spiramycin at 24°C | Gas evolution at 75°C | Liquid formation at 110°C |
|  | | |
| Liquid at 139°C | | |

**Infrared spectroscopy (IR)**

Samples were diluted with a non-absorbing KBr matrix at a 1-5% ratio. DRIFTS were recorded as shown in figure 3.30 with main absorption peaks indicated in table 3.20. The main absorptions for spiramycin recrystallised from acetone compared well with the raw material.

**Table 3.20** Main absorption peaks of spiramycin recrystallised from acetone.

| Main absorptions | Wavenumbers ($cm^{-1}$) |
|---|---|
| 1 | 567.1 |
| 2 | 869.9 |
| 3 | 904.6 |
| 4 | 993.3 |

**Table 3.20** (continued)

| Main absorptions | Wavenumbers ($cm^{-1}$) |
|---|---|
| 5 | 1053.1 |
| 6 | 1161.2 |
| 7 | 1282.7 |
| 8 | 1720.5 |
| 9 | 3466.1 |

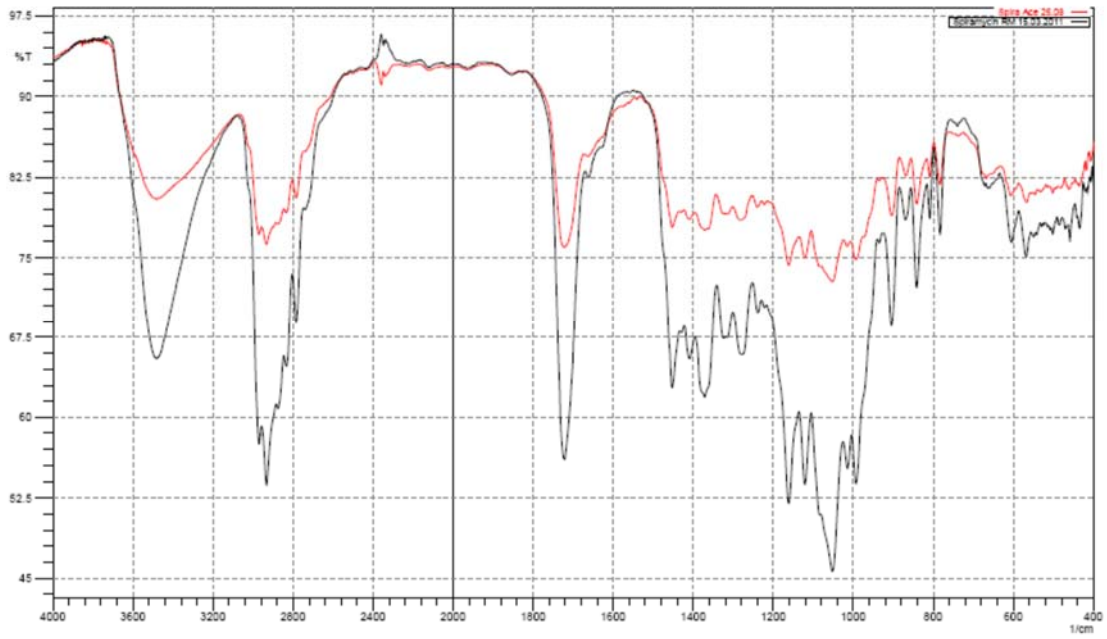


**Figure 3.30** Overlay of the infrared spectra of spiramycin recrystallised from acetone (red) and the raw material (red).

### 3.10.3.2 Acetonitrile (ACN)

**Differential scanning calorimetry (DSC)**

Spiramycin recrystallised from acetonitrile showed mulitiple endothermic peaks starting at approximately 90ºC until all of the residual solvent had been released. At approximately 140ºC the sample starts to degrade (figure 3.31).

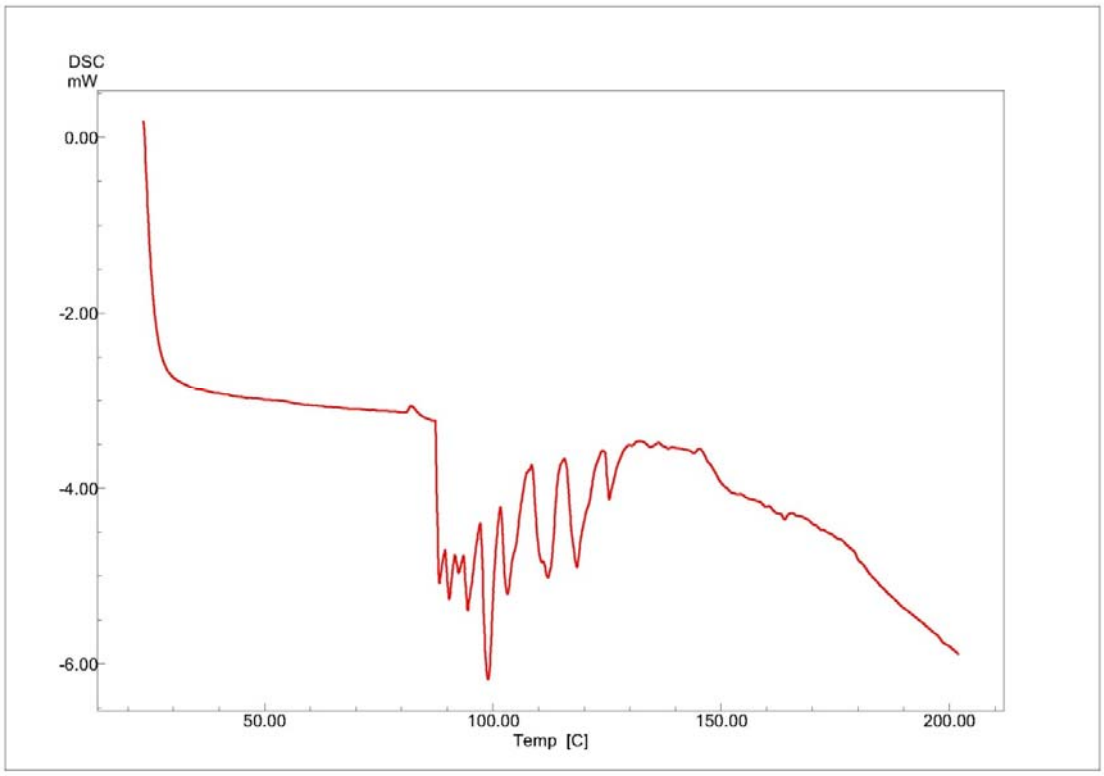


**Figure 3.31** The DSC thermogram of amorphous spiramycin recrystallised from ACN.

**Thermogravimetric analysis (TGA)**

The thermogram (figure 3.32) of spiramycin samples recrystallised from ACN shows a weight loss of approximately 10.4%, in comparison to the theoretical weight loss of 4.6% for a 1:1 spiramycin:ACN solvate.

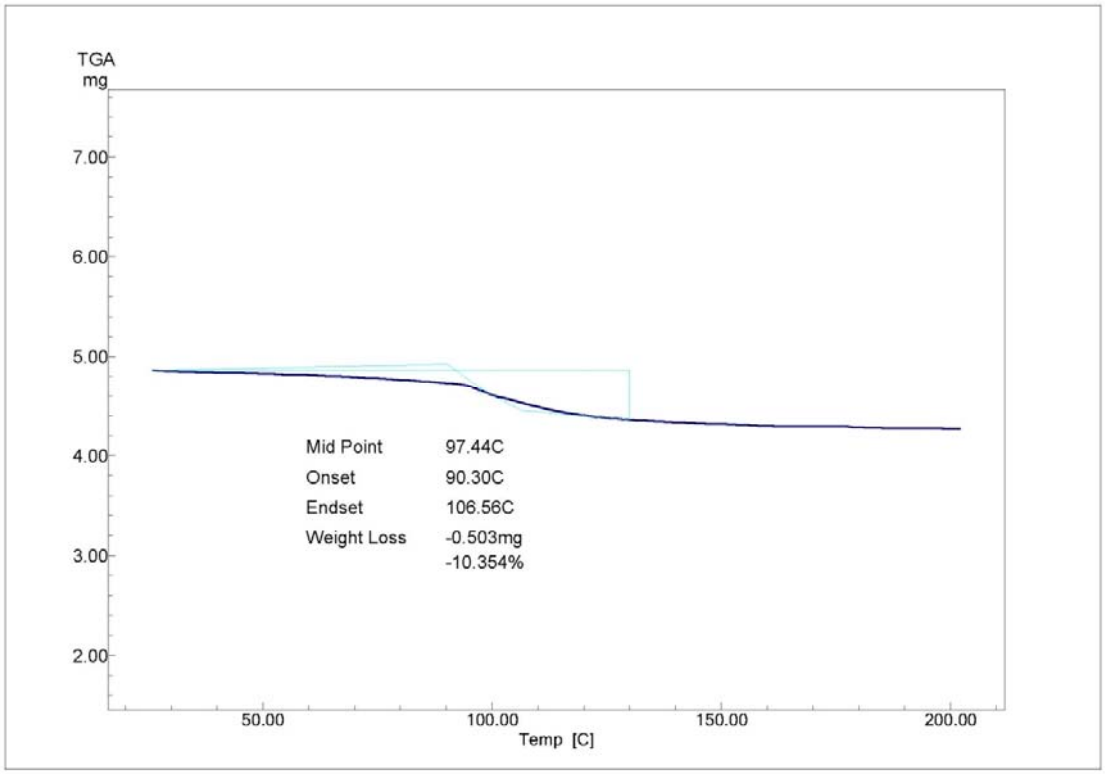


**Figure 3.32** The TGA of spiramycin recrystallised from ACN.

**Thermal microscopy (TM)**

TM micrographs (table 3.21) were taken to observe and clarify thermal events noted in the DSC thermogram over elevated temperatures. The residual solvent released from the sample, noted in the TGA, is confirmed by the gas evolution in the silicone oil.

**Table 3.21** TM results for spiramycin recrystallised from acetonitrile

| | | |
|---|---|---|
| 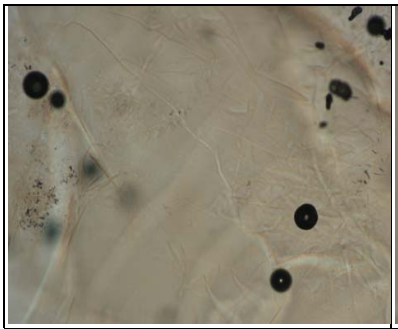 |  | 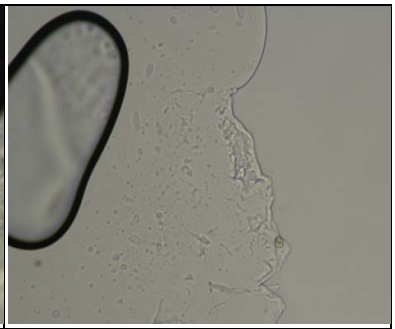 |
| Amorphous spiramycin at 28°C | Gas evolution at 90°C | Transition to the liquid phase at 120°C |

**Table 3.21** (continued)

| |
|---|
| 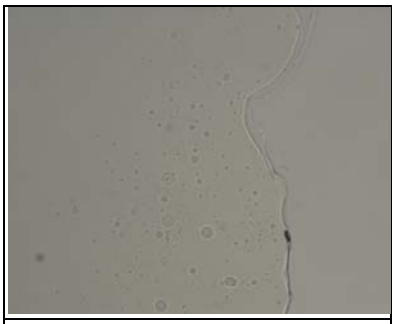 |
| Liquid at 132°C |

**Infrared spectroscopy (IR)**

KBr and a small amount of the sample were carefully ground together and its DRIFTS recorded (figure 3.33). The main absorptions correspond well to that of the raw material.

**Table 3.22** Main absorption peaks of spiramycin recrystallised from acetonitrile.

| Main absorptions | Wavenumbers ($cm^{-1}$) |
|---|---|
| 1 | 568.1 |
| 2 | 868.0 |
| 3 | 903.7 |
| 4 | 994.4 |
| 5 | 1051.3 |
| 6 | 1163.1 |
| 7 | 1280.8 |
| 8 | 1723.5 |

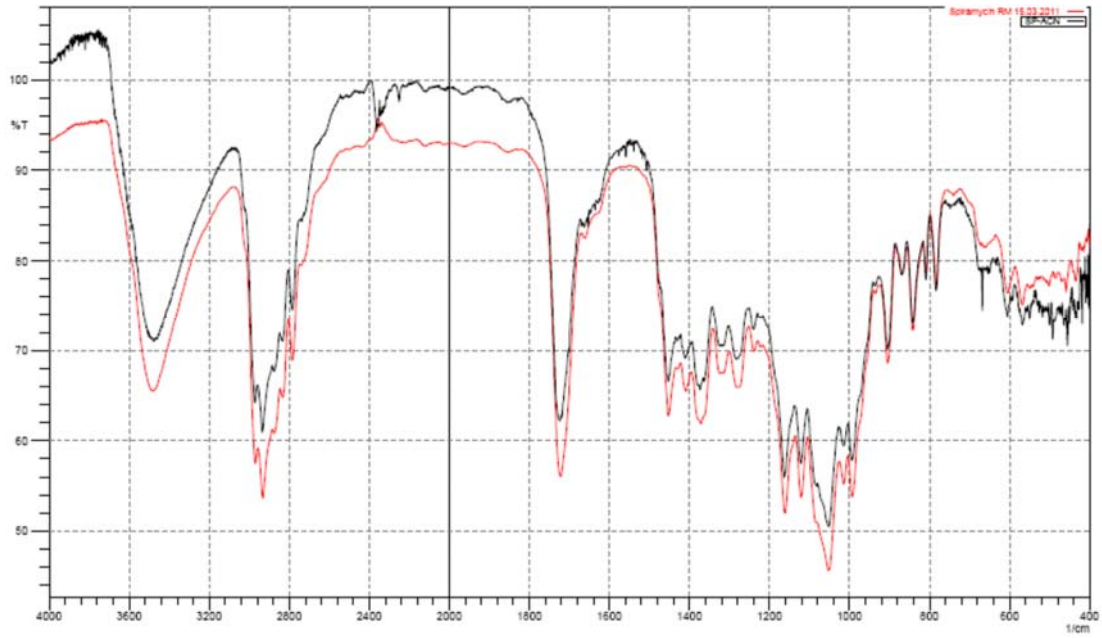


**Figure 3.33** Overlay of spectra of spiramycin recrystallised from ACN (black) and the raw material (red).

### 3.10.3.3 Chloroform

**Differential scanning calorimetry (DSC)**

In the DSC thermogram of chloroform the step change associated with $T_g$ is not clear. It could therefore not be accurately defined (figure 3.34).

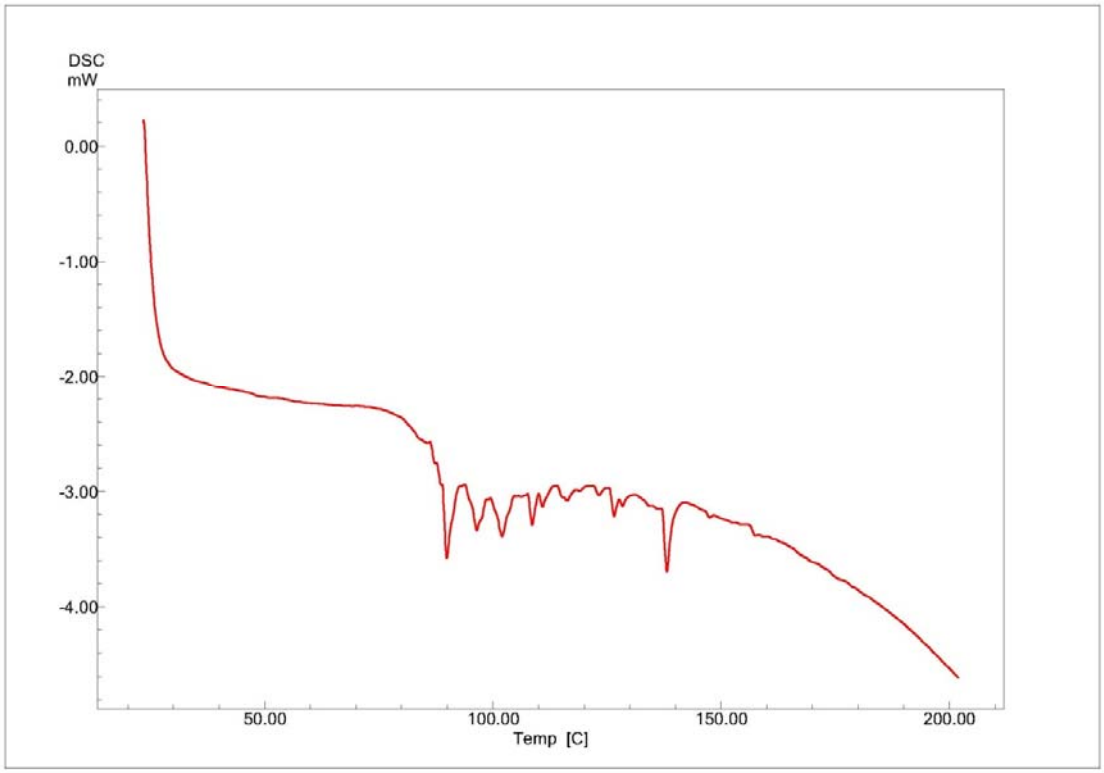


**Figure 3.34** DSC thermogram of spiramycin recrystallised from chloroform.

**Thermogravimetric analysis (TGA)**

Thermogravimetric analysis was performed on spiramycin samples recrystallised from chloroform. The experimental weight loss was 23.3%, compared to theoretical weight loss 12.4% for a 1:1 spiramycin:chloroform solvate (figure 3.35).

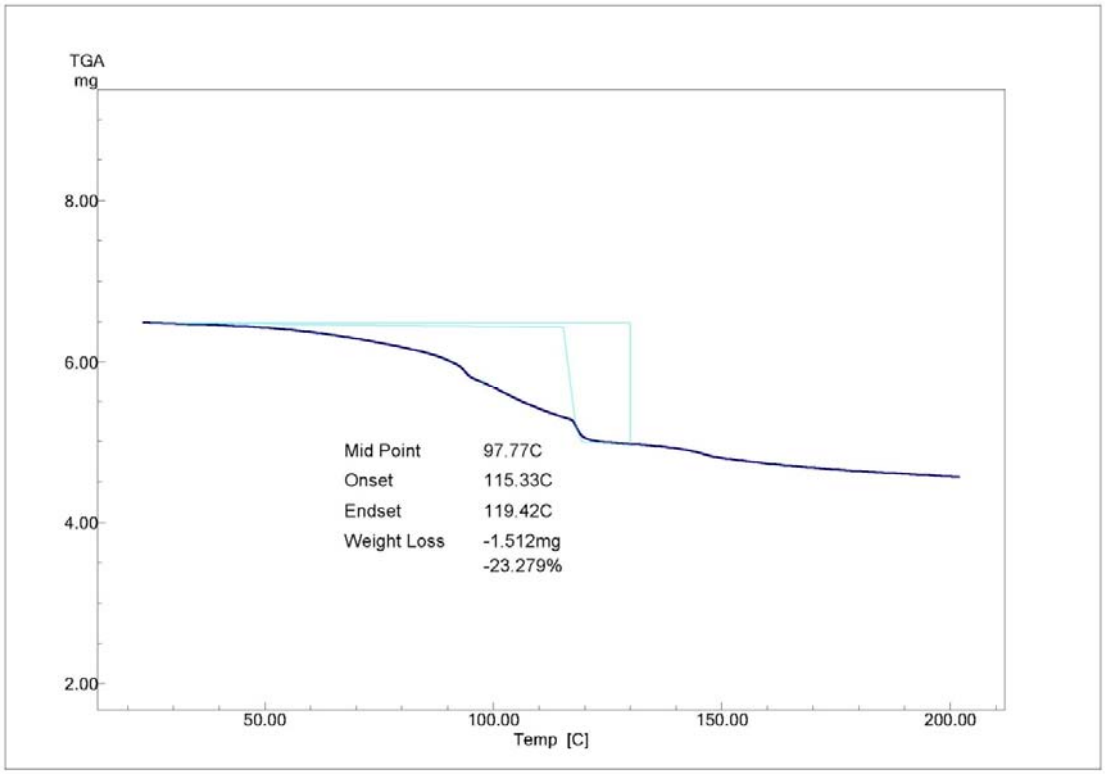


**Figure 3.35** The TGA of spiramycin recrystallised from chloroform.

**Thermal microscopy (TM)**

Table 3.23, shows captured images of amorphous spiramycin and morphological changes to the liquid form as the temperature increases. Solvent evaporation starts at approximately 67ºC.

**Table 3.23** TM results for spiramycin recrystallised from chloroform

| | | |
|---|---|---|
| 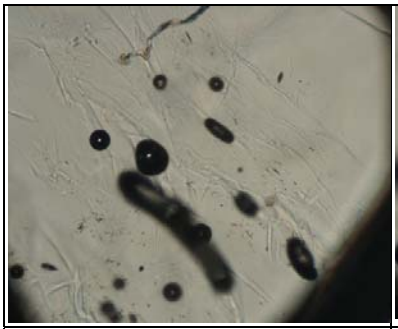 | 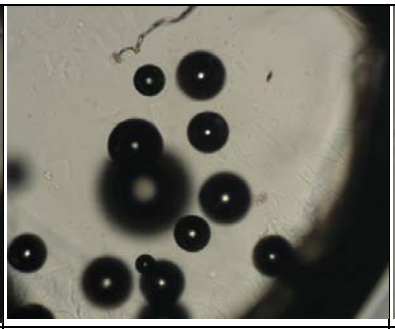 |  |
| Amorphous spiramycin at 23°C | Gas evolution at 67°C | Liquid form at 130°C |

**Infrared spectroscopy (IR)**

The main region of interest in the IR spectrum of spiramycin recrystallised from chloroform is between 2000 $cm^{-1}$ and 2400 $cm^{-1}$. The peaks observed at 2339.7 $cm^{-1}$ and 2358.9 $cm^{-1}$ were not present in the IR spectrum of the raw material (figure 3.36).

**Table 3.24** Main absorption peaks of spiramycin recrystallised from chloroform.

| Main absorptions | Wavenumbers ($cm^{-1}$) |
|---|---|
| 1 | 567.1 |
| 2 | 754.2 |
| 3 | 869.9 |
| 4 | 904.6 |
| 5 | 1053.1 |
| 6 | 1161.2 |
| 7 | 1284.6 |
| 8 | 1726.3 |
| 9 | 2339.7 |
| 10 | 2358.9 |
| 11 | 3475.7 |

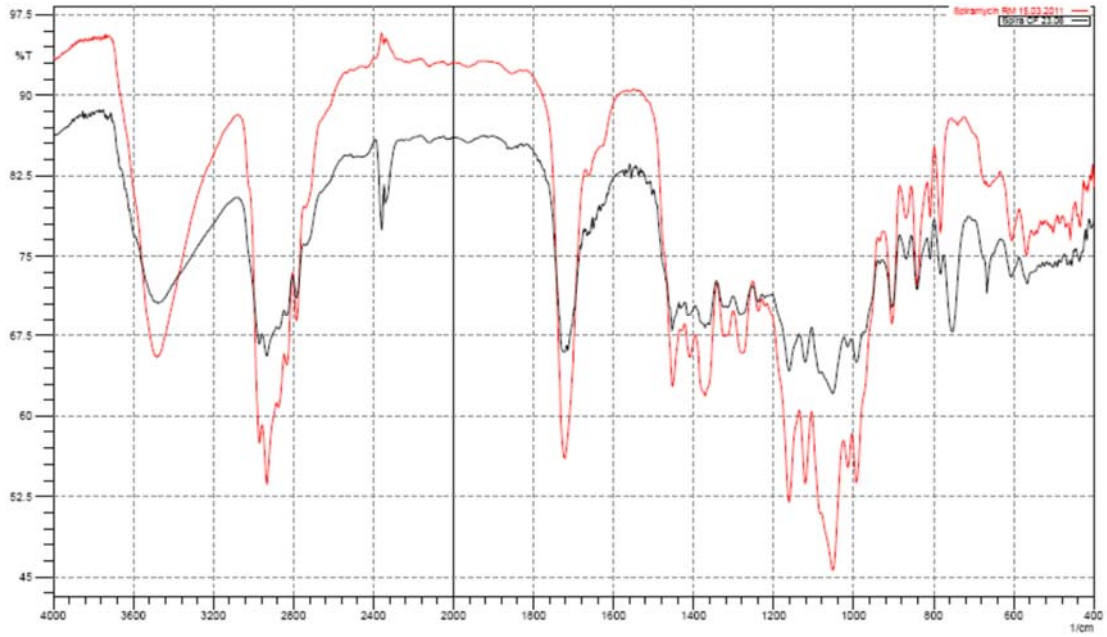


**Figure 3.36** Overlay of the infrared spectra of spiramycin recrystallised from chloroform (black) and the raw material (red).

### 3.10.3.4 Dichloromethane (DCM)

**Differential scanning calorimetry (DSC)**

The DSC thermogram (figure 3.37) of spiramycin recrystallised from dichloromethane exhibits a sharp endothermic peak at 75.6ºC. This is probably due to the release of residual solvent (DCM), if the events observed in the TM are considered.

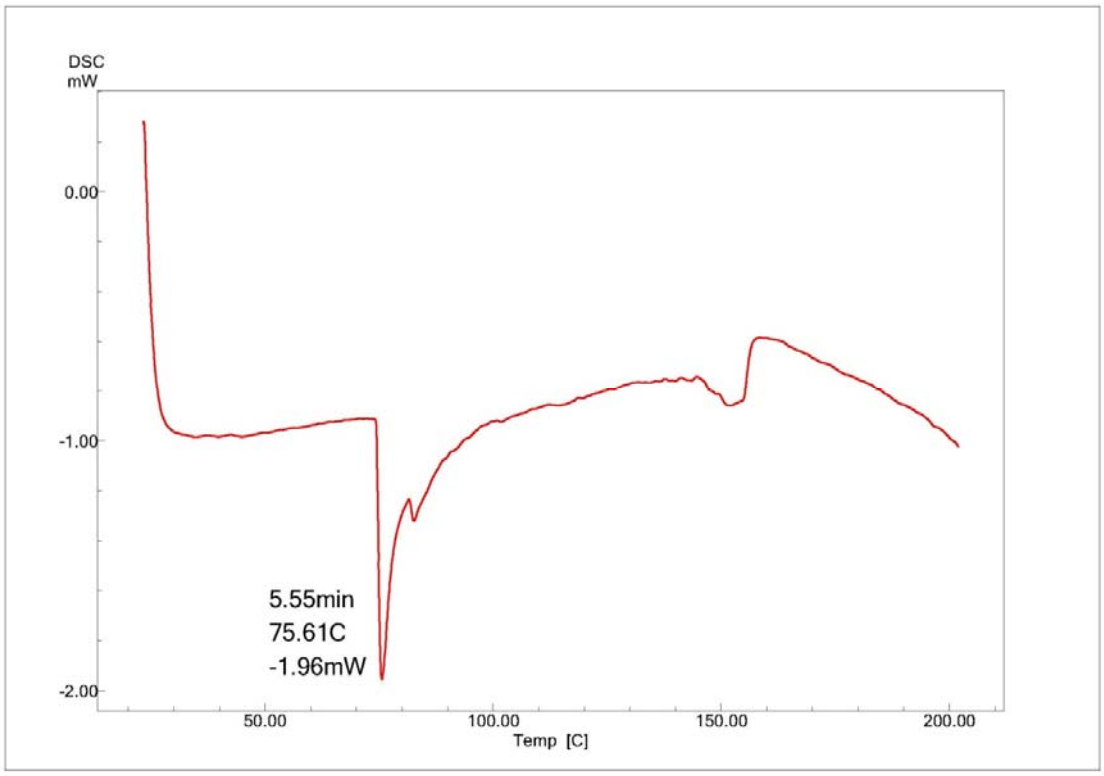


**Figure 3.37** DSC thermogram of spiramycin recrystallised from DCM.

**Thermogravimetric analysis (TGA)**

The 16.3% weight loss indicates excess residual solvent present in the sample, as the theoretical weight loss due to desolvation would be 9.2% for a 1:1 spiramycin: DCM solvate (figure 3.38).

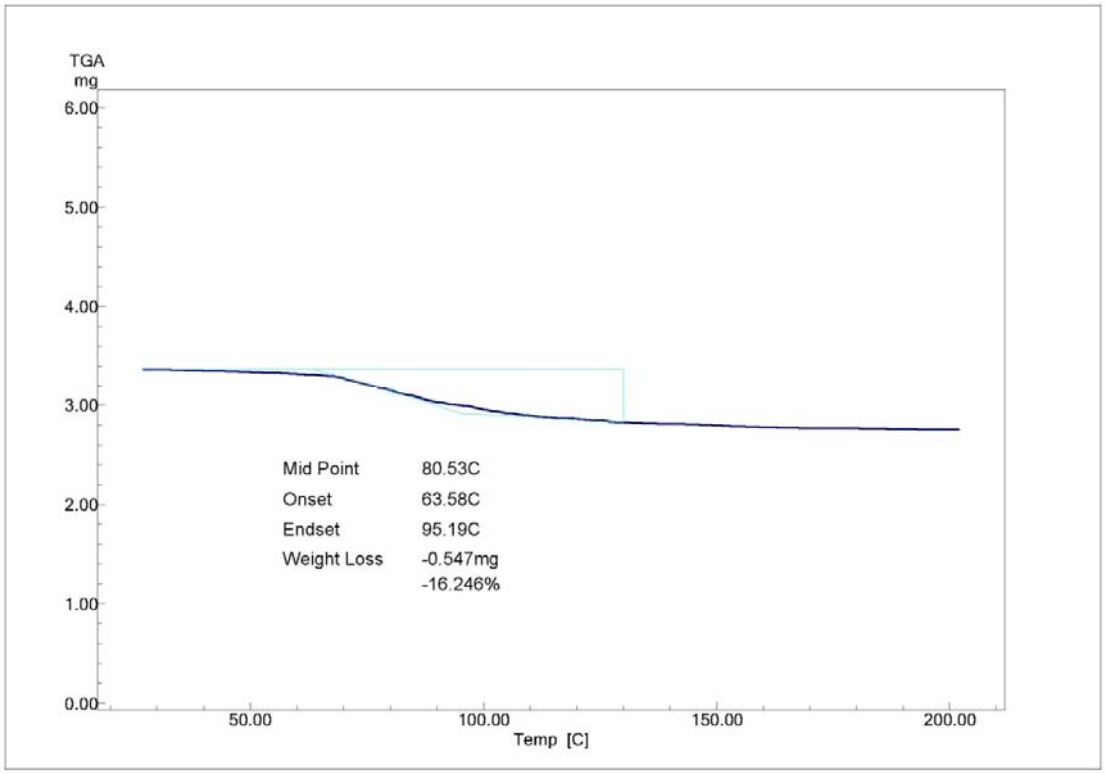


**Figure 3.38** The TGA of spiramycin recrystallised from DCM.

**Thermal microscopy (TM)**

Table 3.25 shows thermal events captured throughout the different stages of heating.

**Table 3.25** TM results for amorphous spiramycin recrystallised from DCM

| | | |
|---|---|---|
| 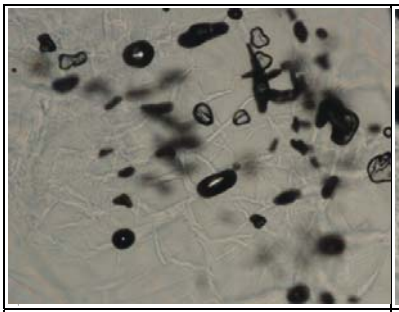 |  | 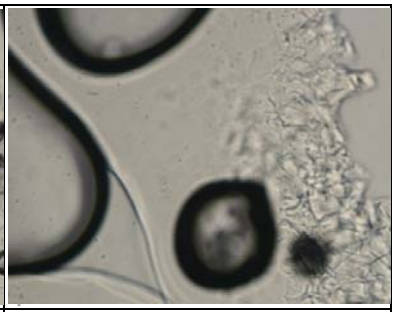 |
| Amorphous spiramycin at 27.4°C | Gas evolution starting at 72°C | Transition to the liquid state at 112.5 |

**Table 3.25** (continued)

| |
|---|
| 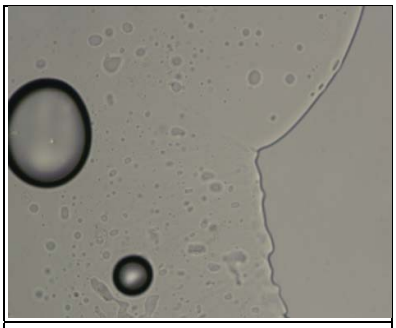 |
| Liquid at 129°C |

**Infrared spectroscopy (IR)**

DRIFTS were recorded as shown in figure 3.39 with main absorption peaks indicated in table 3.26. The infrared spectrum of spiramycin recrystallised from DCM compared well to that of the material

**Table 3.26** Main absorption peaks of spiramycin recrystallised for DCM.

| Main absorptions | Wavenumbers ($cm^{-1}$) |
|---|---|
| 1 | 567.1 |
| 2 | 868.4 |
| 3 | 905.6 |
| 4 | 1050.3 |
| 5 | 995.3 |
| 6 | 1160.2 |
| 7 | 1273.1 |
| 8 | 3470.1 |

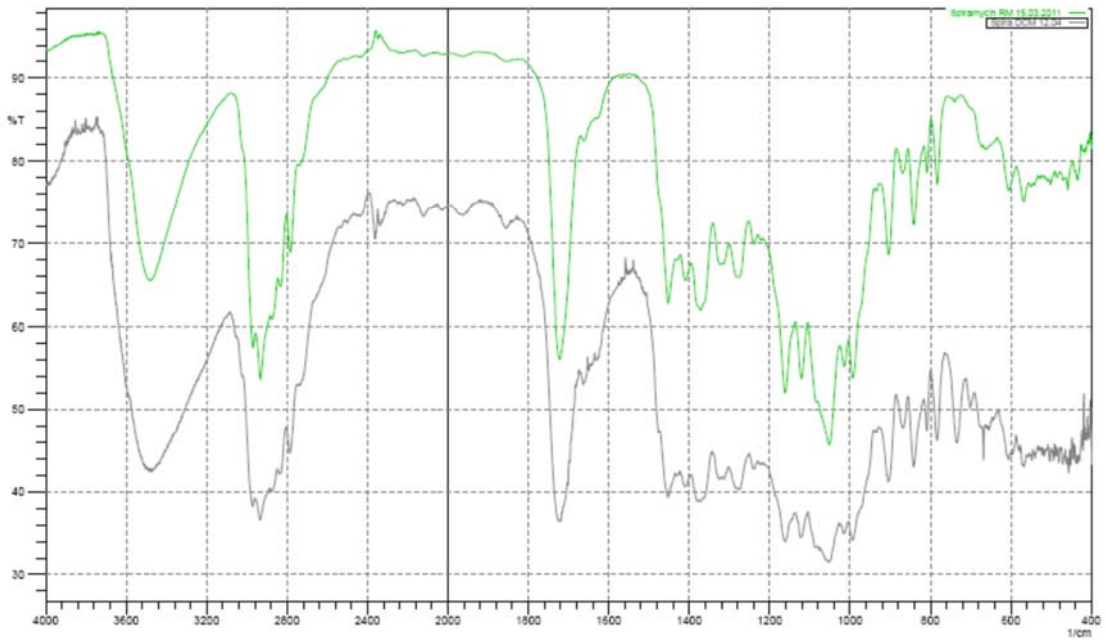


**Figure 3.39** Overlay of the infrared spectrum of spiramycin recrystallised from DCM (grey) and the raw material (green).

### 3.10.3.5 1, 4-dioxane (DXN)

**Differential scanning calorimetry (DSC)**

Figure 3.40 illustrates the thermal events of the sample associated with the application of the heat signal. From approximately 100ºC to 140ºC various thermal events are once again visible which are presumably, as mentioned previously, associated with a combination of factors including structural relaxation and evaporation of solvent, dissolution of spiramycin in released solvent followed by sample degradation, rendering the exact value of the $T_g$ difficult to quantify.

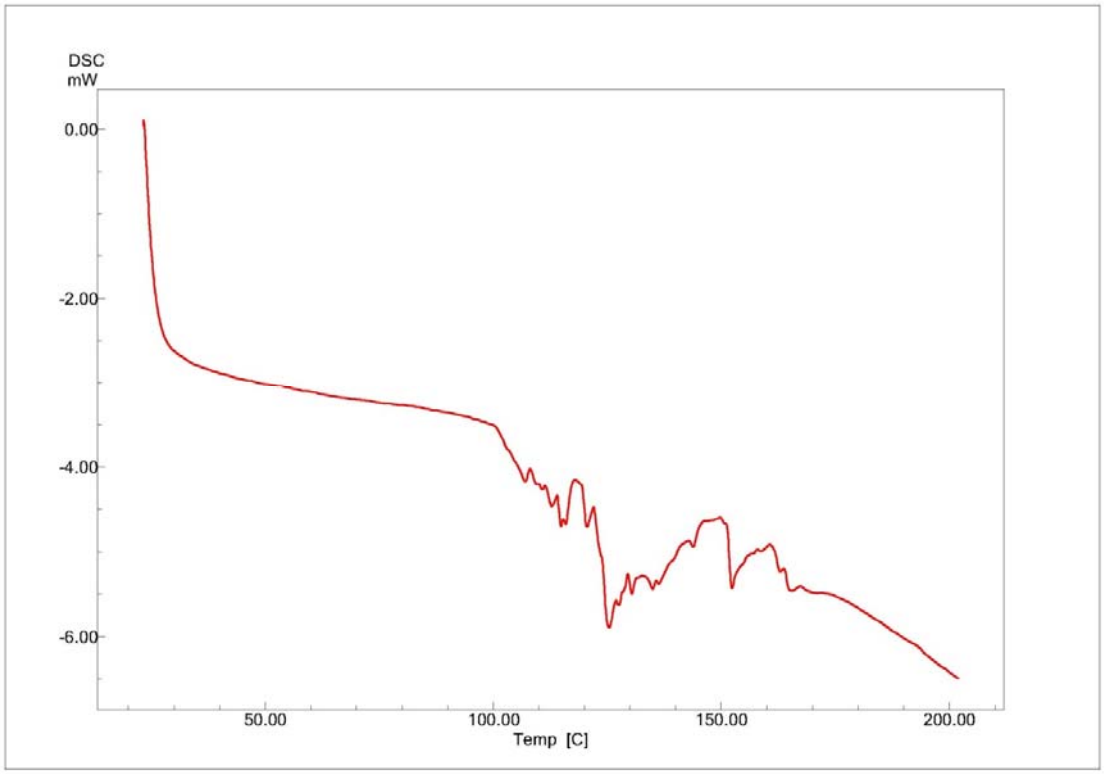


**Figure 3.40** DSC thermogram of spiramycin recrystallised from DXN.

**Thermogravimetric analysis (TGA)**

The experimental weight loss of 10.9% is indicative of the recrystallisation solvent being released from the sample matrix of the recrystallising agent (DXN). Theoretically the weight loss for a 1:1 spiramycin: DXN solvate due to desolvation is 9.5%.

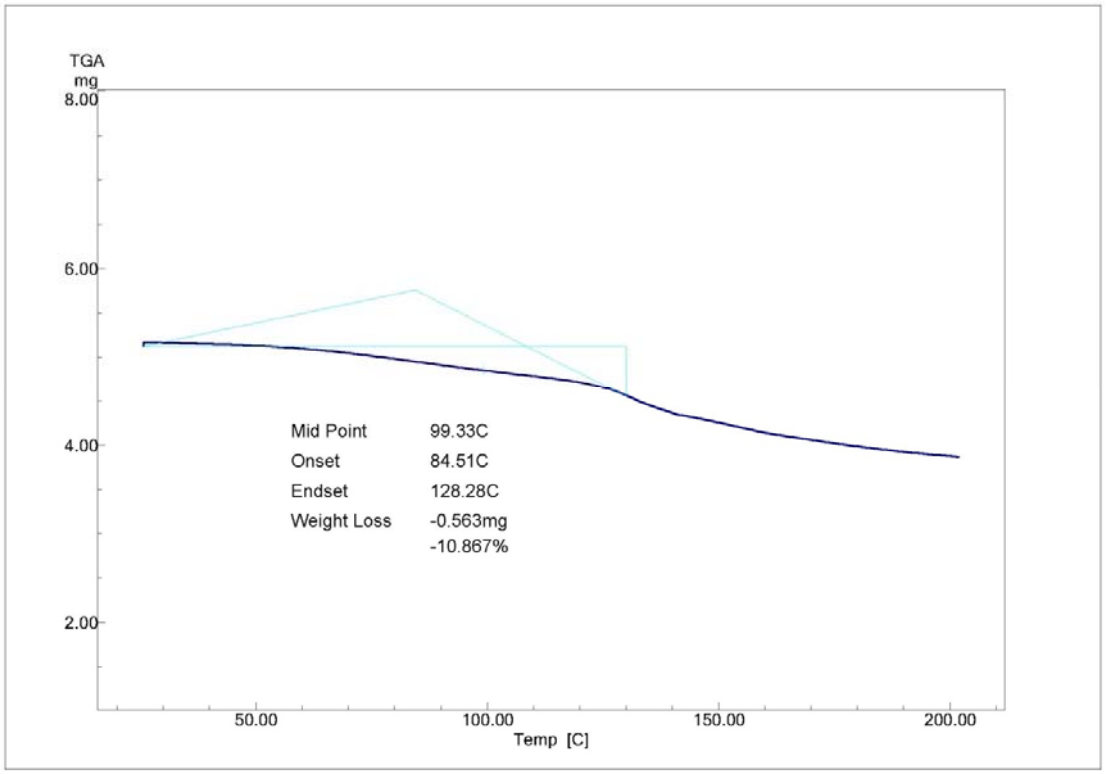


**Figure 3.41** The TGA of spiramycin recrystallised from DXN.

**Thermal microscopy (TM)**

The captured micrographs show the initial sample, an amorphous substance, converting to a fluid-like state upon application of heat.

**Table 3.27** TM results for spiramycin recrysallised from DXN

| | | |
|---|---|---|
| 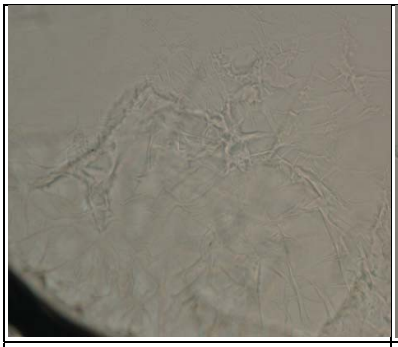 | 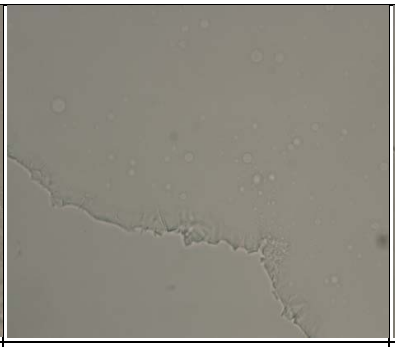 | 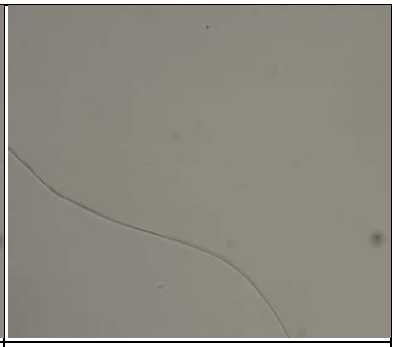 |
| Amorphous spiramycin at 26°C | Liquid formation at 108°C | Liquid formation at 128ºC |

**Infared spectroscopy (IR)**

DRIFTS were recorded as shown in figure 3.42 with main absorption peaks indicated in table 3.26. The main region of interest in the IR spectrum (figure 3.42) of spiramycin recrystallised from DXN is between 2000 $cm^{-1}$ and 2400 $cm^{-1}$. The peaks observed at 2341.6 $cm^{-1}$ and 2358.9 $cm^{-1}$ were not present in the IR spectrum of the raw material.

**Table 3.26** Main absorption peaks of spiramycin recrystallised for DXN.

| Main absorptions | Wavenumbers ($cm^{-1}$) |
|---|---|
| 1 | 567.1 |
| 2 | 873.8 |
| 3 | 904.6 |
| 4 | 993.3 |
| 5 | 1051.2 |
| 6 | 1161.2 |
| 7 | 1726.3 |
| 8 | 1953.9 |
| 9 | 1979.0 |
| 10 | 2341.6 |
| 11 | 2358.9 |
| 12 | 3475.3 |

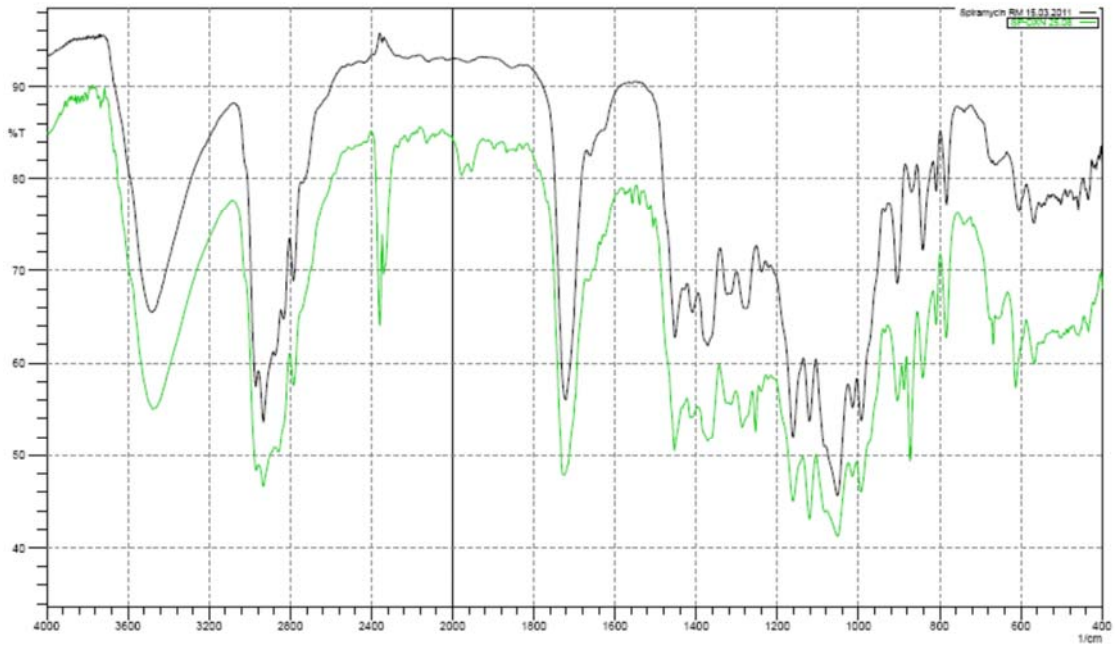


**Figure 3.42** The infared spectra of spiramycin recrystallised from DXN (green) and the raw material (black).

### 3.10.3.6 Ethyl acetate (EA)

**Differential scanning calorimetry (DSC)**

The DSC indicates several endothermic events from approximately 90ºC to 140ºC where after the sample appears to undergo degradation (figure 3.43).

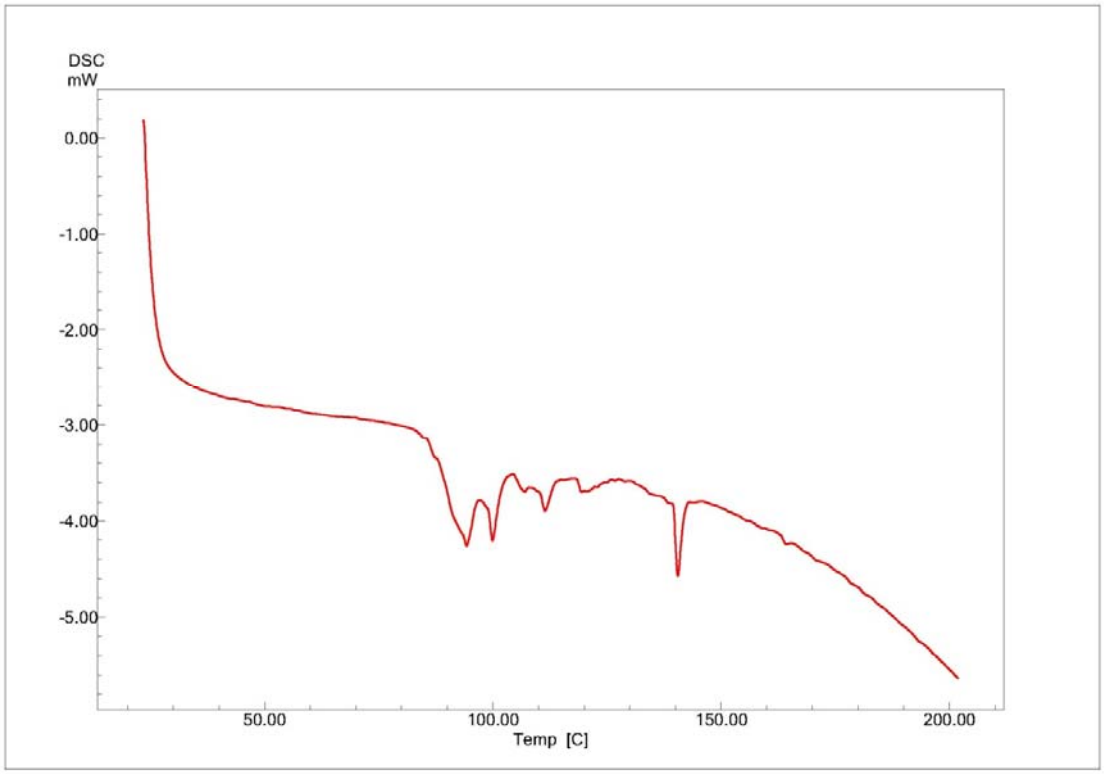


**Figure 3.43** DSC thermogram of spiramycin recrystallised from EA.

**Thermogravimetric analysis (TGA)**

The weight loss measured was 13.3% and indicative of entrapped solvent within the structure of the sample matrix. The theoretical weight loss calculated for a 1:1 spiramycin: EA solvate is 9.5%.

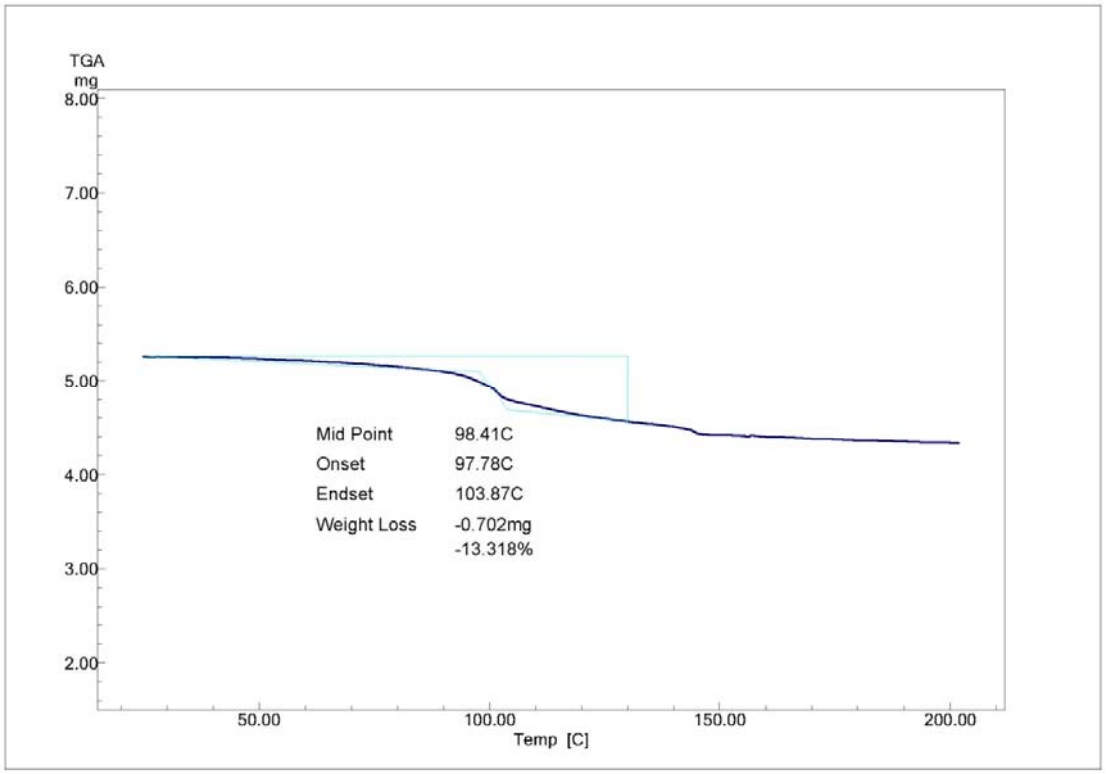


**Figure 3.44** The TGA of spiramycin recrystallised from EA.

**Thermal microscopy (TM)**

TM photographs show the change from a solid into a liquid. Gas evolution is observed as the entrapped recrystallising solvent is released from the sample upon the application of heat.

**Table 3.27** TM results for spiramycin recrystallised from EA

| | | |
|---|---|---|
| 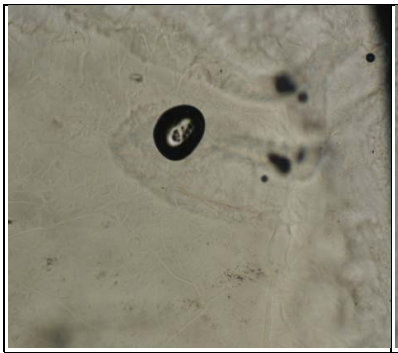 | 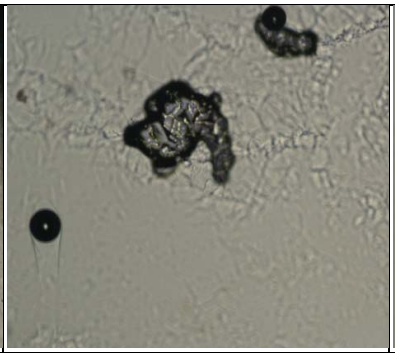 |  |
| Sample at 25ºC | Liquid formation at 115ºC | Liquid at 124ºC |

**Infrared spectroscopy (IR)**

DRIFTS were recorded as shown in figure 3.45 with main absorption peaks indicated in table 3.28. The main region of interest in the IR spectrum of spiramycin recrystallised from EA between 2000 $cm^{-1}$ and 2400 $cm^{-1}$. The peaks observed at 2339.7 $cm^{-1}$ and 2358.9 $cm^{-1}$ were not present in the IR spectrum of the raw material.

**Table 3.28** Main absorption peaks of spiramycin recrystallised for EA.

| Main absorptions | Wavenumbers ($cm^{-1}$) |
|---|---|
| 1 | 567.1 |
| 2 | 868.0 |
| 3 | 904.6 |
| 4 | 993.3 |
| 5 | 1053.1 |
| 6 | 1161.2 |
| 7 | 1275.0 |
| 8 | 1724.4 |
| 9 | 2339.7 |
| 10 | 2358.9 |
| 11 | 3475.7 |

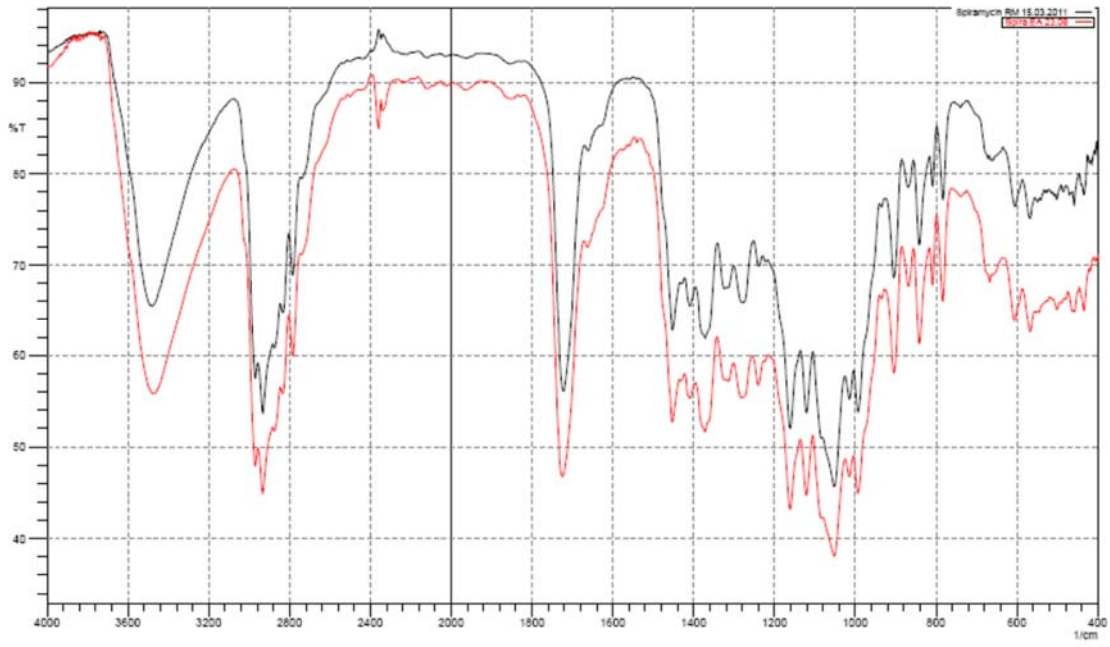


**Figure 3.45** Overlay of the infrared spectra of spiramycin recrystallised from EA (red) and the raw material (black).

### 3.10.3.7 Tetrahydrofuran (THF)

**Differential scanning calorimetry (DSC)**

Figure 3.46 shows a complex thermogram with an intricate pattern of thermal events, most of which are assumed to be associated with solvent evaporation from the surface and from within the sample matrix.

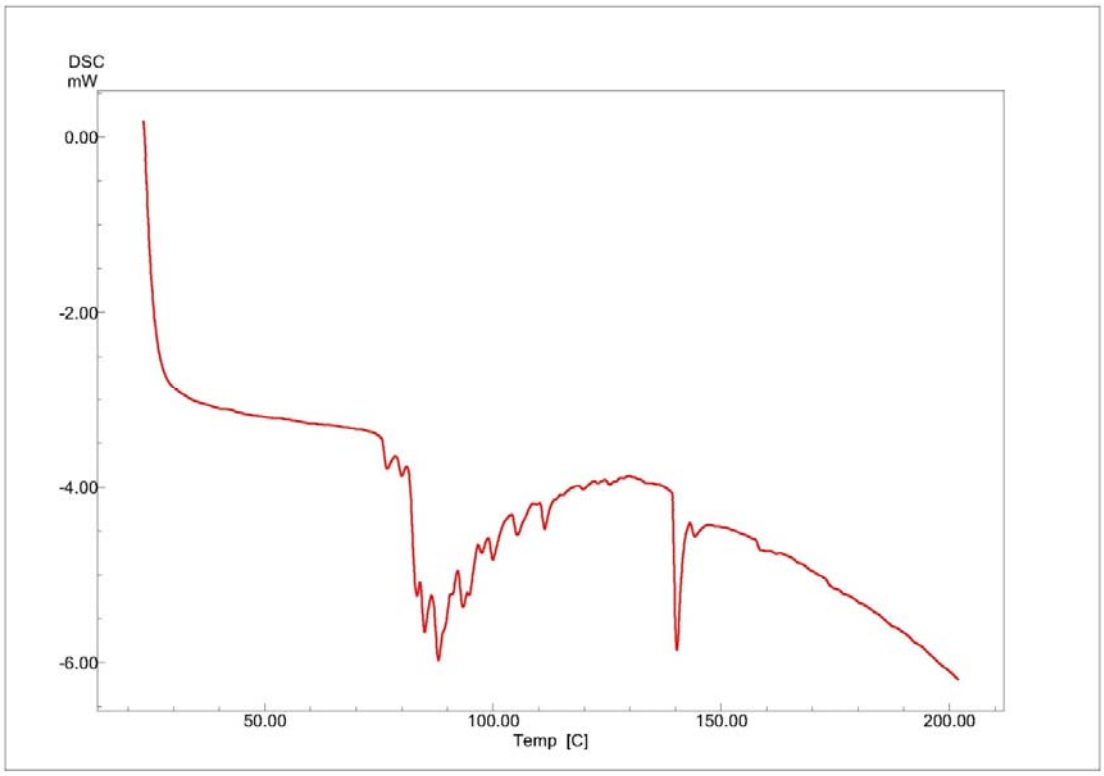


**Figure 3.46** DSC thermogram of spiramycin recrystallised from THF.

**Thermogravimetric analysis (TGA)**

Theoretical weight loss for a 1:1 spiramycin:THF solvate was calculated as 7.9%, while the results indicate a weight loss of 13.8% (figure 3.47).

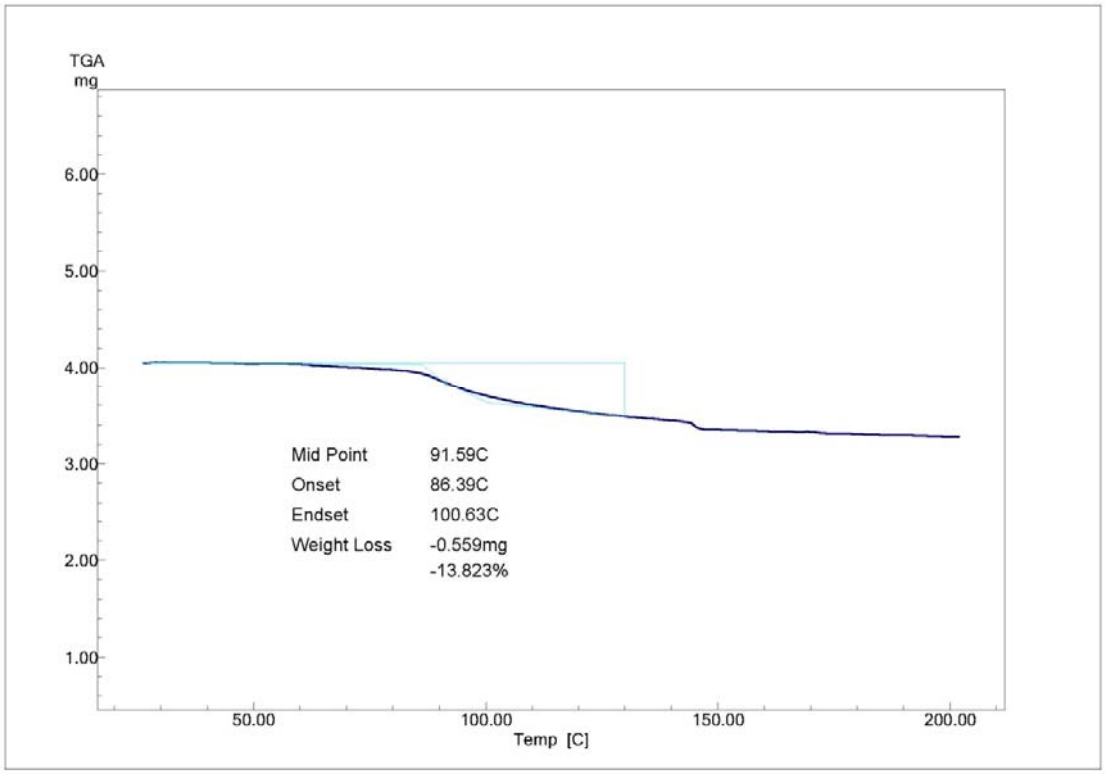


**Figure 3.47** The TGA of spiramycin recrystallised from THF.

**Thermal microscopy (TM)**

Table 3.29 shows the changes in the sample in response to the addition of heat.

**Table 3.29** TM results for spiramycin recrystallised from THF

| | | |
|---|---|---|
|  |  |  |
| Amorphous spiramycin at 23°C | Cracks appearing at 72°C | Transition to the liquid form at 86°C |

**Table 3.29** (continued)

| |
|---|
| 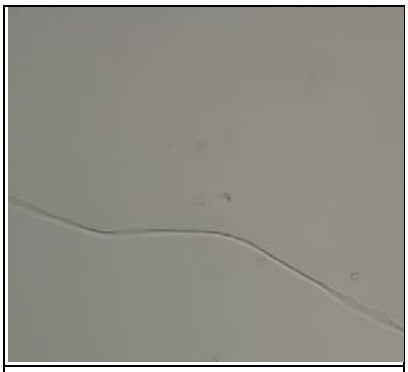 |
| Liquid at 140°C |

**Infrared spectroscopy (IR)**

DRIFTS were recorded as shown in figure 3.48 with main absorption peaks indicated in table 3.30. The peaks observed at 2341.6 $cm^{-1}$ and 2358.9 $cm^{-1}$ were not registered in the IR spectrum of the raw material.

**Table 3.30** Main absorption peaks of spiramycin recrystallised for THF.

| Main absorptions | Wavenumbers ($cm^{-1}$) |
|---|---|
| 1 | 567.1 |
| 2 | 868.0 |
| 3 | 904.6 |
| 4 | 993.3 |
| 5 | 1053.1 |
| 6 | 1161.2 |
| 7 | 1726.3 |
| 8 | 2341.6 |
| 9 | 2358.9 |
| 10 | 3470.4 |

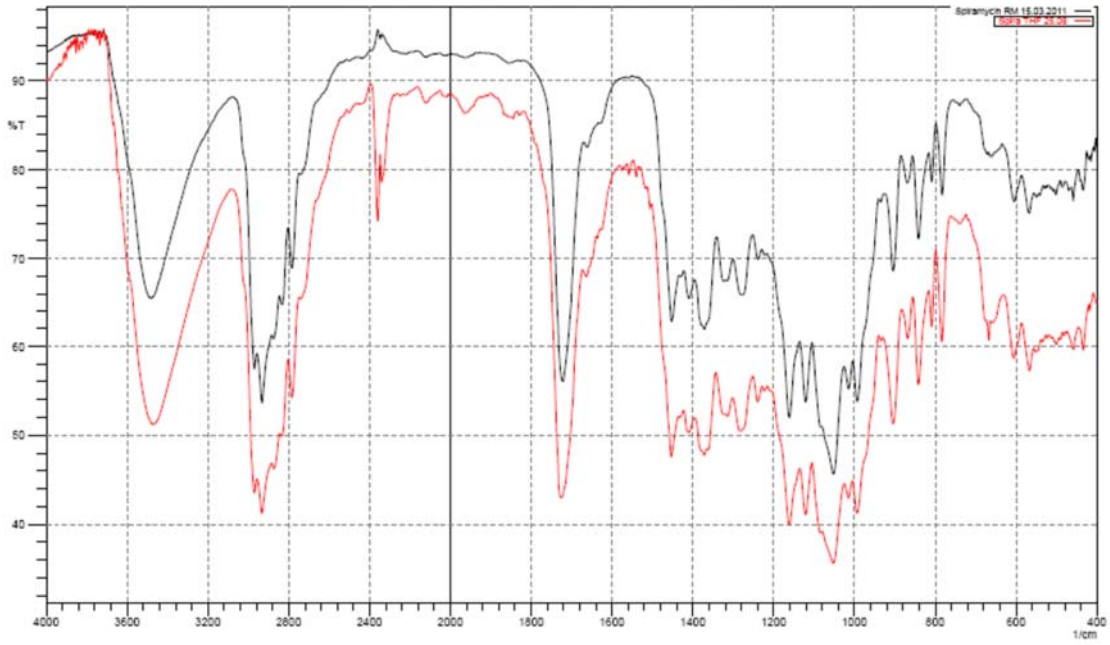


**Figure 3.48** Overlay of the infrared spectra of spiramycin recrystallised from THF (red) and the raw material (black).

### 3.10.3.8 Toluene

**Differential scanning calorimetry (DSC)**

Unlike the other DSC thermograms, thermal events only appear after 100ºC. However, the same perplexity is noted as with all of the other samples (figure 3.49).

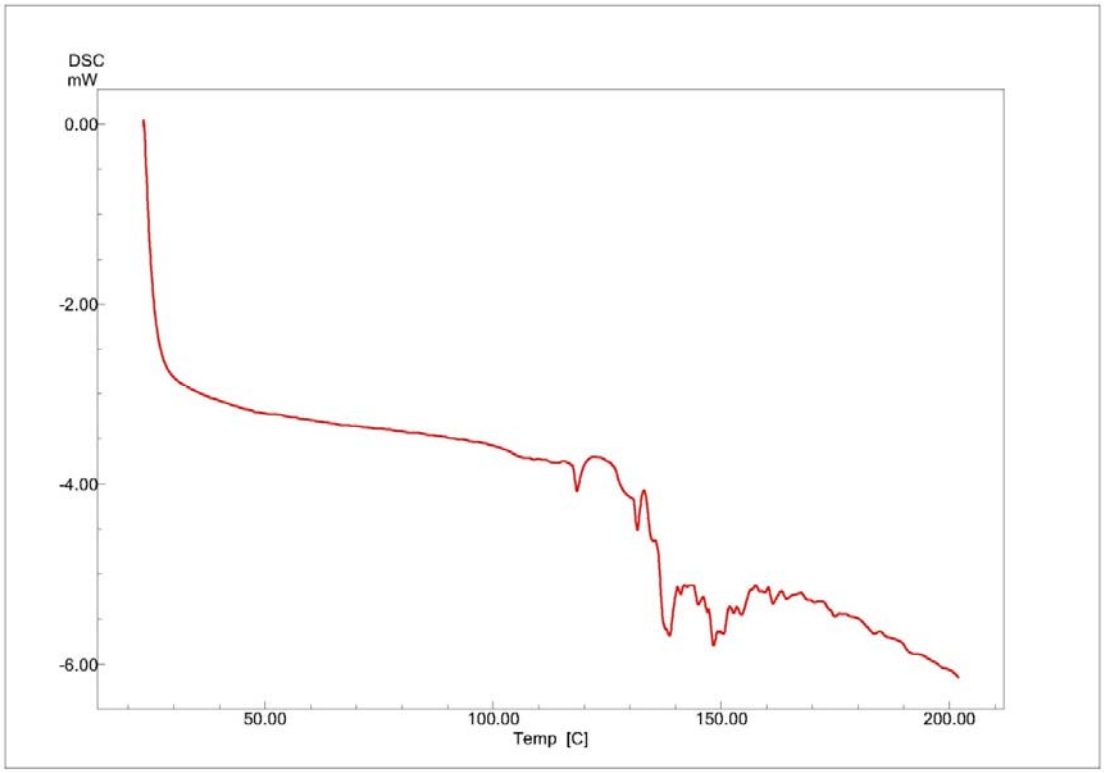


**Figure 3.49** DSC thermogram of spiramycin recrystallised from toluene.

**Thermogravimetric analysis (TGA)**

Theoretical weight loss for a 1:1 spiramycin: toluene solvate was calculated to be 9.9%, whilst the experimental weight loss was 8.4% (figure 3.50).

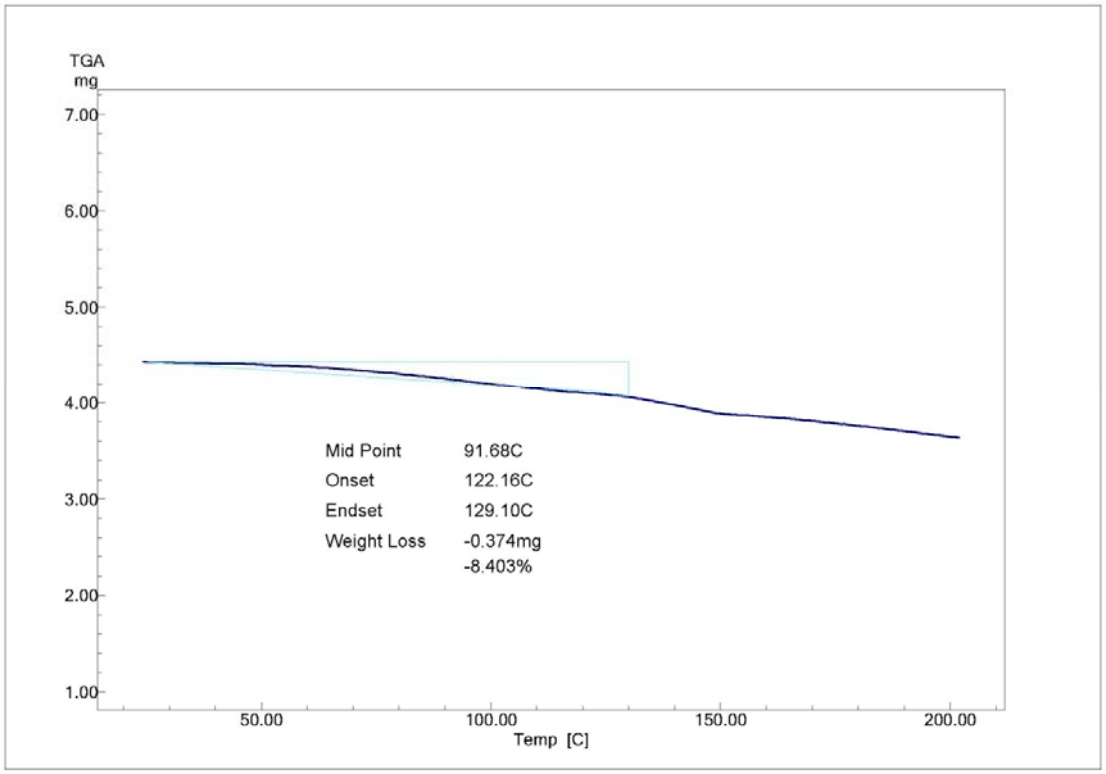


**Figure 3.50** The TGA of spiramycin recrystallised from toluene.

**Thermal microscopy (TM)**

Table 3.31 summarises the results for the sample exposed to a hot-stage microscope over an elevated temperature range.

**Table 3.31** TM results for spiramycin recrystallised from toluene

| | | |
|---|---|---|
|  |  |  |
| Amorphous spiramycin at 21°C | Transition to the liquid phase starting at 82°C | Liquid at 106°C |

**Infrared spectroscopy (IR)**

DRIFTS were recorded as shown in figure 3.51 with main absorption peaks indicated in table 3.32. The main absorptions for spiramycin recrystallised from toluene were similar to that of the raw material.

**Table 3.32** Main absorption peaks of spiramycin recrystallised for toluene

| Main absorptions | Wavenumbers ($cm^{-1}$) |
|---|---|
| 1 | 567.1 |
| 2 | 868.0 |
| 3 | 903.7 |
| 4 | 993.4 |
| 5 | 1163.1 |
| 6 | 1280.8 |
| 7 | 1724.4 |
| 8 | 3473.8 |

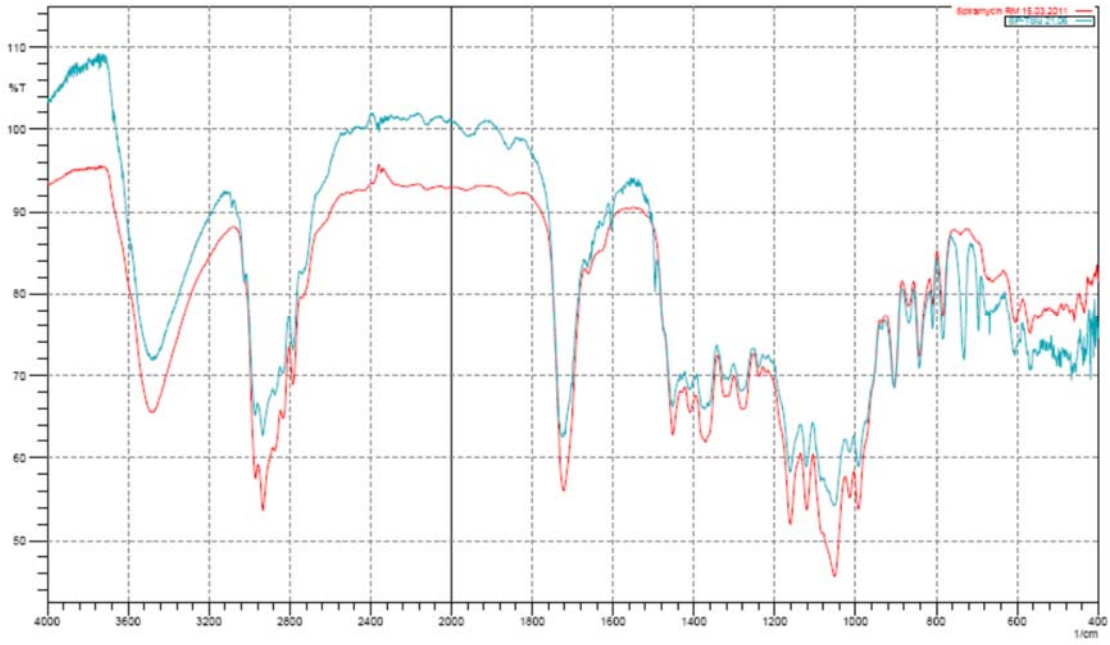


**Figure 3.51** Overlay of the infrared spectra of spiramycin recrystallised from toluene (blue) and the raw material (red).

### 3.10.3.8 Discussion of the results generated from diverse solvents

The results from the thermal analysis show that this form of assessment is not a functional approach to characterise this complex macromolecular antibiotic since it will be very difficult to clarify each of the numerous thermal events observed in the DSC traces (figure 3.54). The results from XRPD and IR were much less speculative compared with the thermal analysis results. Definitive similarities or differences could be pointed out; the IR patterns of spiramycin recrystallised from acetone, acetonitrile, dichloromethane and toluene all resembled the IR pattern of the raw material. As with the alcohol group differences in the region of 2000-4000 $cm^{-1}$ were once again noted with chloroform, 1,4-dioxane, ethyl acetate and tetrahydrofuran having distinct peaks that were not present with the raw material (figure 3.52). XRPD patterns were, however, all similar to one another which reflected the results from the alcohol group (figure 3.53).

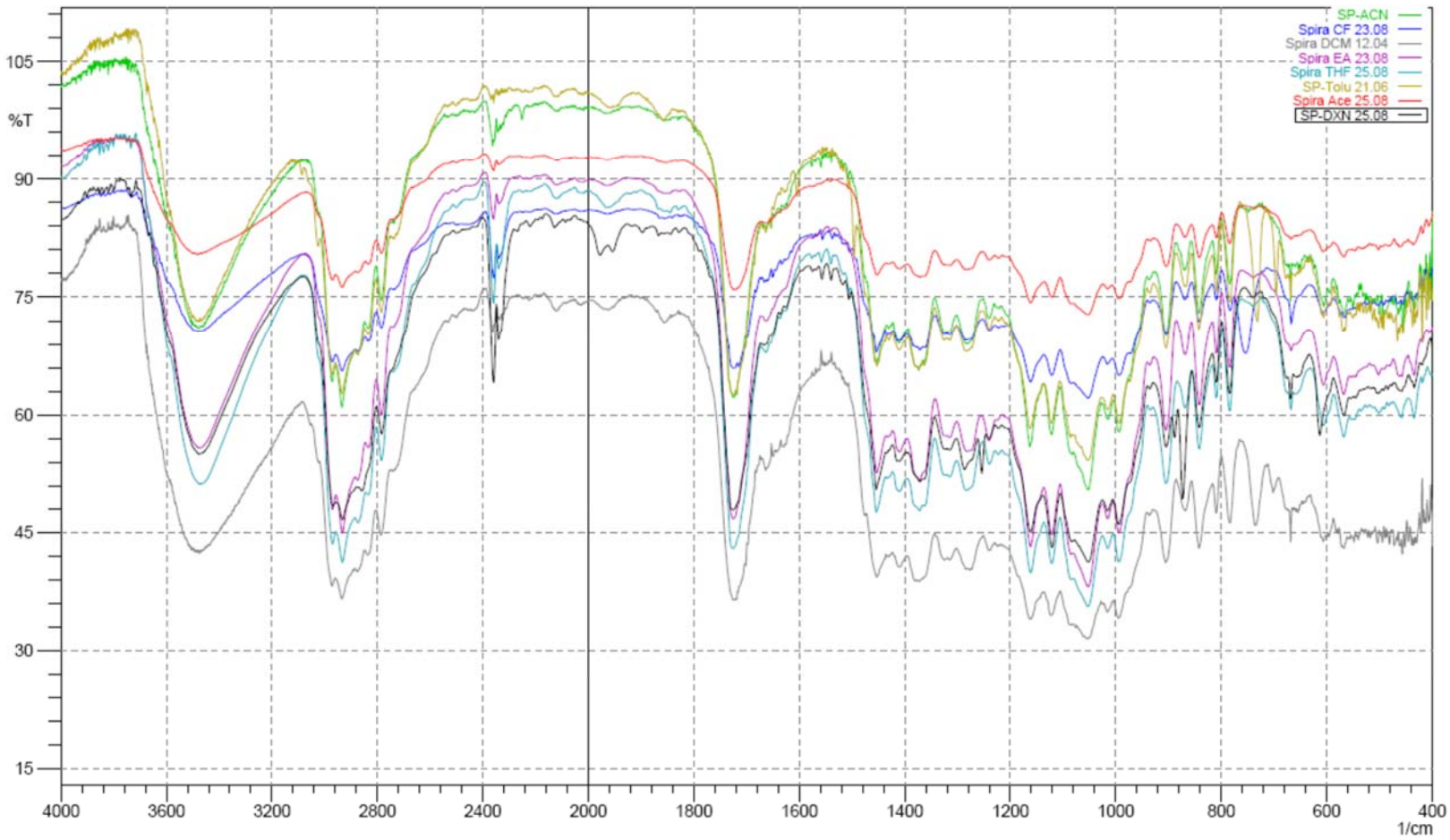


**Figure 3.52** Overlay of the infrared spectrum of spiramycin recrystallised from the diverse solvent group.

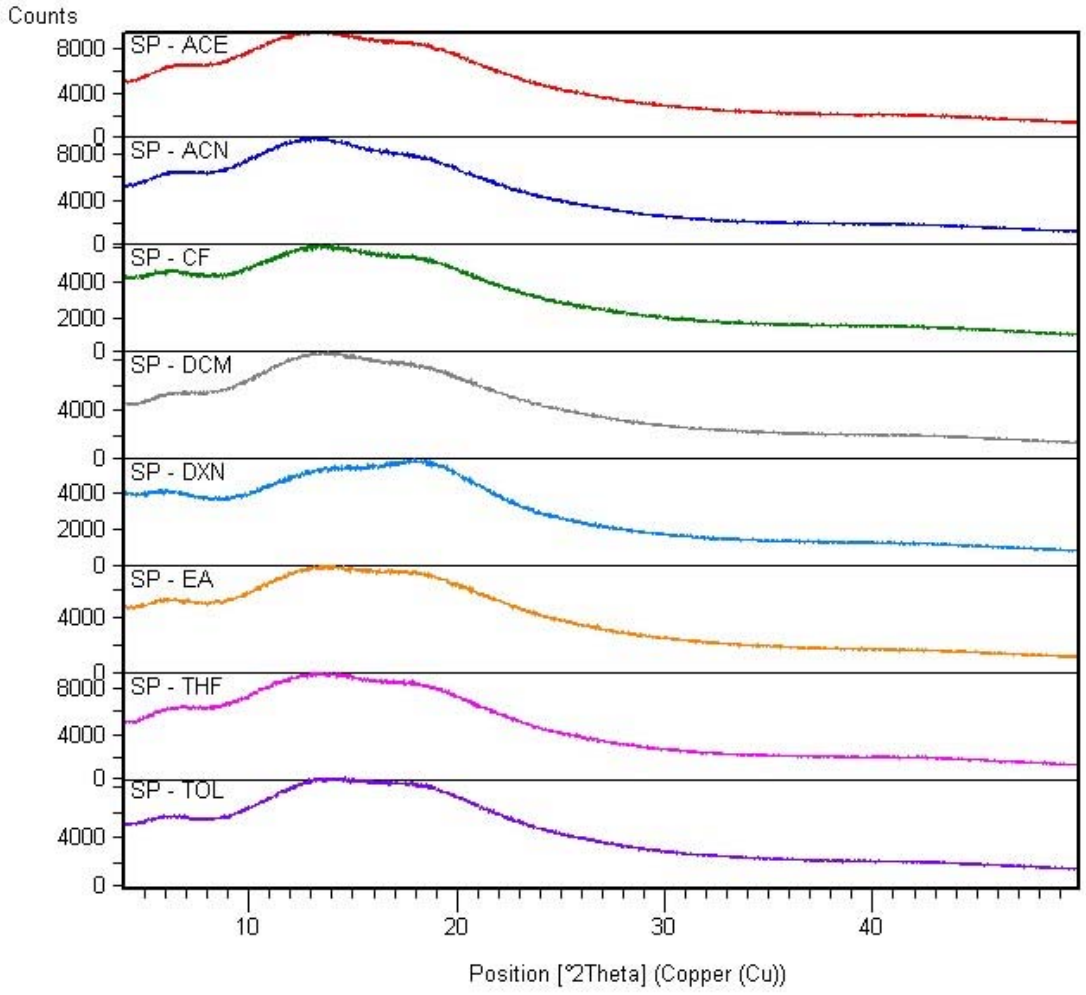


**Figure 3.53** Stack graph showing the amorphous XRPD patterns for samples generated from the diverse solvent group.

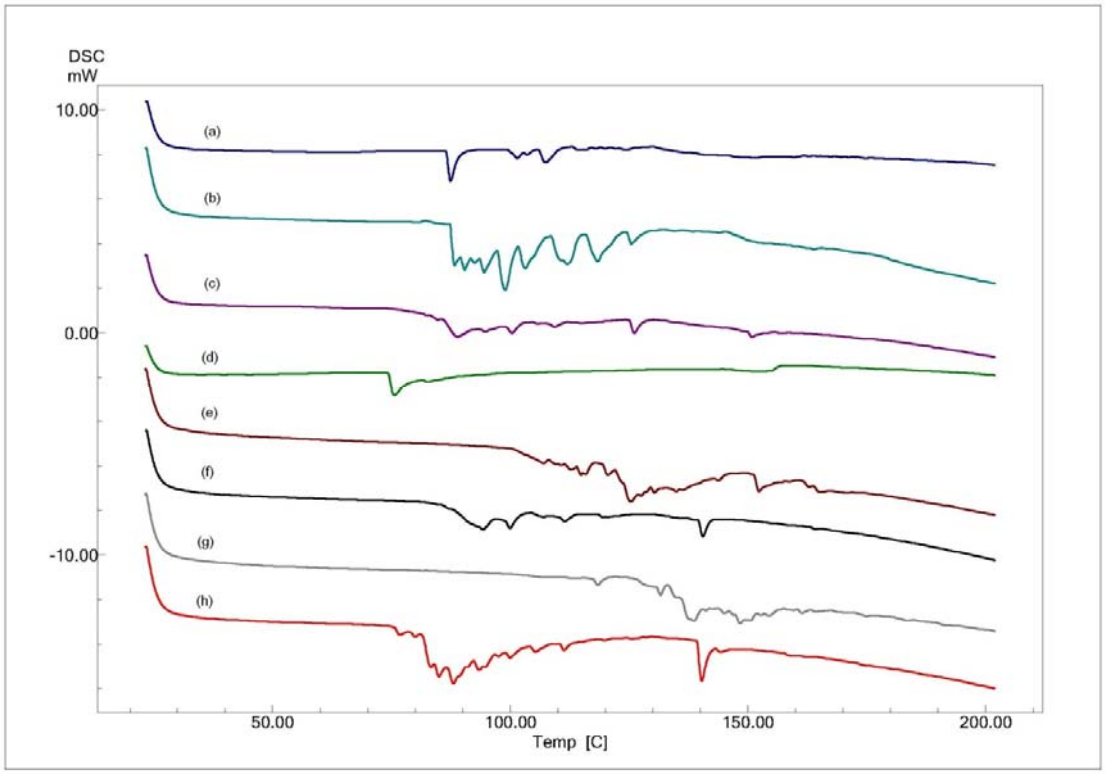


**Figure 3.54** Overlay of the DSC thermograms of spiramycin recrystallised from the diverse solvent group: (a) acetone (b) acetonitrile (c) chloroform (d) dichloromethane (e) 1,4-dioxane (f) ethyl acetate (g) tetrahydrofuran (h) toluene.

### 3.11 Solubility studies

Most of the macrolide group of antibiotics have poor water soluble characteristics. The solubility of a drug substance is considered one of the most important physico-chemical properties. The bioavailability of drugs administered orally is primarily dependent on its solubility in the gastro-intestinal fluids and its permeability across the gastro-intestinal barriers. For a drug to be transported across the biological membranes, it needs to be present in a dissolved form. Therefore, a drug with poor solubility can delay or limit drug absorption, having a direct influence on the potency or bioavailability of oral dosage forms (Rao *et al.,* 2009).

Studies were conducted on powdered samples of spiramycin raw material and the recrystallisation products obtained from DCM and ACN. The solubility tests were performed as described in chapter 2, section 2.9.

### 3.11.1 Results

**Table 3.33** Solubility test results of spiramycin recrystallised from dichloromethane (SP-DCM) and acetonitrile (SP-ACN) with the raw material as reference (SP-RM)

| Test tube | Concentration (ug/ml) | | |
|---|---|---|---|
| | **SP-RM** | **SP-DCM** | **SP-ACN** |
| **1** | 28.540 | 20.797 | 26.505 |
| **2** | 27.390 | 22.398 | 23.365 |
| **3** | 24.862 | 19.680 | 22.204 |
| **4** | 26.220 | 19.940 | 24.875 |
| **5** | 25.120 | 21.123 | 21.229 |
| **Average** | 26.427 | 20.788 | 23.636 |
| **sd** | 1.549 | 1.078 | 2.102 |
| *Abbreviation:* sd = standard deviation | | | |

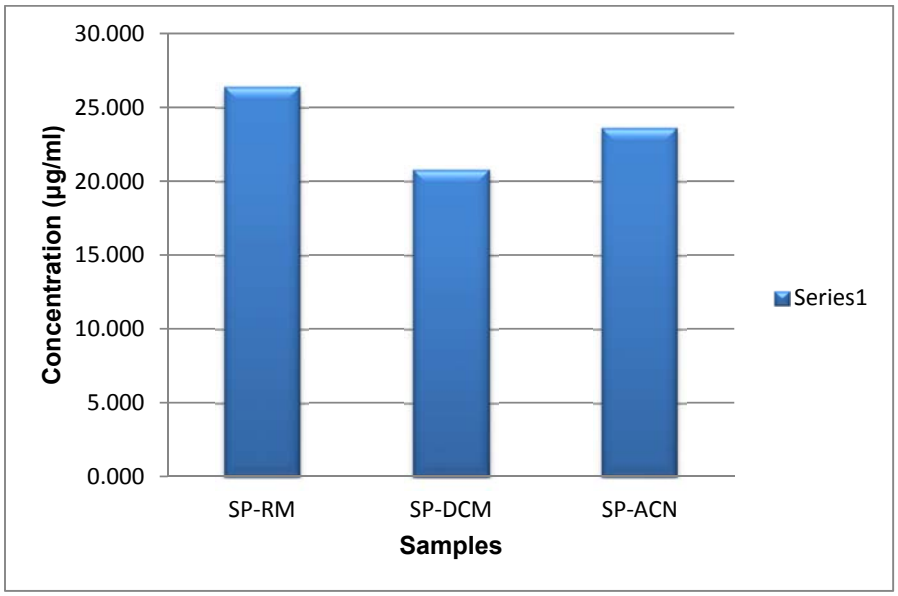


**Figure 3.55** A comparison of the solubility of the amorphous forms generated from dichloromethane (SP-DCM) and acetonitrile (SP-ACN) with the raw material (SP-RM) as reference.

### 3.11.2 Discussion of the solubility data

The solubility results indicate that samples generated from dichloromethane and acetonitrile are less soluble in water than the raw material. This could be due to a number of factors; including poor wettability properties or particle-particle interactions. In addition, structural relaxation associated with annealing of the sample could also have contributed to the lower solubility, since this phenomenon is associated with a lowering in the overall potential energy of the substance. A lower potential energy level means greater stability, and is therefore less soluble. Also the recrystallisation products from ACN and DCM could be more crystalline than the amorphous raw material. The XRPD diffractograms show that all the recrystallisation products were amorphous, but the degree of amorphism was not quantified. Amorphous material tends to be more soluble than crystalline products.

### 3.12 Conclusion

The recrystallisations from different solvents did not yield any crystalline products. The goal of producing new polymorphic forms was therefore not achieved. Only amorphous products were generated, probably because the raw material itself was amorphous and due to the morphology of the particles, with solvent easily being trapped in pores.

As one would expect, the non-equilibrium nature of the amorphous product, and in particular those that contained residual solvent, not only made the handling of samples difficult but also greatly influenced the experimental consistency. In fact the use of thermal methods were not particularly useful tools in the analysis of this particular macro molecular antibiotic, since substantial sample to sample variations were mostly obtained. This is in line with the statement of Bird (1994): "The techniques (DSC and TGA) are of little practical value for these compounds [amoxicillin trihydrate and amoxicillin sodium]". The thermal analysis results should therefore not be seen as negative with respect to equivalence. Craig *et al.* (1999) proposed that characterisation studies be conducted on cooling cycles for the sake of reproducibility, as the liquid form is in an equilibrium state at the beginning of the experiment. The fact that most of the samples were binary mixtures, containing both the original material and the solvent, meant that such a heating cycle would remove the solvent, changing the overall composition of the sample, which would ultimately defeat the purpose.

Crystallographic and spectroscopic methods were used for the structural elucidation of the samples. These methods proved much more efficient in terms of experimental reproducibility and quality. Samples generated from 2-butanol, chloroform, ethyl acetate, 1.4-dioxane, methanol, n-propanol, iso-propanol and tetrahydrofuran showed characteristic peaks in the range of 2000-2400 $cm^{-1}$ that were not present in the IR spectrum of the raw material. Conversely, the XRPD patterns were all identical, exhibiting a characteristic "halo" pattern with no detectable Bragg diffraction peaks.

Solubility results conducted on selected amorphous samples, indicated less favourable water solubility profiles, which can either be prescribed to poor wettability, particle-particle interactions or the effects of annealing.

Cui (2007) argued that most modern techniques including the use of thermal and spectroscopic techniques and methods that aim to detect the bulk properties of an amorphous substance, lead to "systemic inaccuracy" since the heterogeneous nature of the drug substance means that some molecules have higher energy levels than the bulk

average. It should be a challenge to develop suitable characterisation methods to determine accurately the thermodynamic stability of amorphous APIs on a molecular level.